Synthesis & characterization of yttria-stabilised zirconia (YSZ) hollow fibre support for Pd based membrane

By

Tshamano Matamela Bridget

Supervisor: Prof Martin Onani

Co-supervisor: Prof Bernard Bladergroen

A thesis submitted in fulfilment of the degree of Masters of Science in the Department of Chemistry, Faculty of Natural Science, University of the Western Cape

October 2013

Declaration

I declare that this thesis is my own, unaided work. It has not been submitted before for any degree or examination in any other University.

_____

(Signature of candidate)

_____ Day of _____ 2013

Acknowledgements

Firstly, I would like to express my deepest gratitude to God for His Blessing and for giving me an ability and strength to complete this project.

Special thanks to Dr M Onani and Prof B Bladergroen for their expert guidance, valuable suggestions and enthusiastic support during the research and through the course of my study. Their fruitful ideas throughout the research project have helped me complete this work successfully.

I would also like to extend my sincere appreciation to my family, especially to my ever-loving parents and brothers who are always on my side, Thank you for the support and the encouragement you gave me to pursue my dreams.

I would like to thank HySA/Systems for offering me the opportunity, the facility to do research and the financial support.

May God bless all of us and only HE, the Almighty could repay all my debts to all of you.

Abstract

Inorganic based membranes which have a symmetric/asymmetric structure have been produced using an immersion induced phase inversion and sintering method. An organic binder solution (dope) containing yttria-stabilised zirconium (YSZ) particles is spun through a triple orifice spinneret to form a hollow fibre precursor, which is then sintered at elevated temperatures to form a ceramic support. The phase inversion process for the formation of hollow fibre membranes was studied in order to produce the best morphological structure/support for palladium based membranes. The spinning parameters, particle size, non-solvent concentration, internal coagulant as well as the calcination temperature were investigated in order to determine the optimum values. Sintering temperature was also investigated, which would yield a sponge-like structure with an optimized permeability, while retaining a smooth outer surface. The supports produced by phase inversion were characterized in terms of dimension by mercury porosimetry, compressed air permeability, Surface Electron Microscopy (SEM) and Atomic Force Microscopy (AFM). The morphology of the produced ceramic support showed either dense or porous characteristics governed by the dynamics of the phase inversion process.

The particle size of YSZ was examined in order to decrease the amount of agglomerates in the spinning suspension. Zetasizer tests indicated that at 15 minutes, the ultrasonic bath effectively homogenised the YSZ particles and prohibited soft agglomerates from reforming in the spinning suspension. In this study, an increase in air gap had no noticeable effect on the finger like voids but it had a considerable effect on both the inner diameter (ID) and outer diameter (OD) of the green fibres, while an increase in bore liquid flow rate and extrusion pressure promoted viscous fingering and significant effect on the ID and OD of the fibres, respectively. There was a decrease in porosity and permeability with increasing sintering temperature, addition of water concentration in the spinning suspension and varying N-methylpyrrolidone (NMP) aqueous solution of the internal coagulant. The amount of YSZ added to the starting suspension influenced the properties of the support structure. Viscous deformation was observed for dope with lower particle loading thus resulted in the formation of cracks and defects during sintering.

Table of Contents

List of Figures

List of Tables

List of Symbols

DESCRIPTION	SYMBOL	UNITS
Concentration	C	mol/m^3
Density	ρ	kg/m^3
Diameter	Φ	cm
Enthalpy	H	kJ/kg
Gas constant	R	J/gmolK
Permeation	F	$\mu mol/m^2Pas^2$
Length	L	cm
Mass	m	grams
Moles	n	mol
Pressure	p	Pa
Surface area	SA	cm^2
Temperature	T	K
Time	t	min or sec
Velocity	υ	m/s
Viscosity	μ	Pa s
Volume	V	L or ml

Abbreviation

Al_2O_3	aluminum oxide
AFM	atomic force microscopy
CeO_2	cerium dioxide
CH_4	methane
CO	carbon monoxide
CO_2	carbon dioxide
CVD	chemical vapour deposition
ED	electrodialysis
ELP	electroless plating
ESD	electrical swing adsorption
FESEM	field emission scanning electron microscopy
GDC	Gd-doped ceria
HFM	hollow fibre membrane
H_2	hydrogen
ID	Inner diameter
IE	Ion- exchange
NMP	N-methylpyrrolidone
O_2	oxygen
OD	outer diameter
PAN	polyacrylonitrile
Pd	palladium
PCS	porous ceramic supports
PES	polyethersulfone
PMS	porous metal supports
PSA	pressure swing adsorption
PSS	porous stainless steel
PVGS	porous vycor glass supports
PVP	polyvinylpyrrolidone
SEM	scanning electron microscopy
SMR	steam methane reforming
TEM	transmission electron microscopy
TEOS	tetraethoxysilane
TiO_2	titanium dioxide

TSA	temperature swing adsorption
WGS	water gas shift
YSZ	yttria-stabilised zirconia

Chapter 1

1. Background

The steady depletion of fossil fuels reserves has led to some comprehensive development in finding alternative energy resources. Hydrogen has recently attracted attention as a possible alternative energy carrier to relieve environmental problems derived from fossil fuel use. The demand for hydrogen is expected to rise in the coming years, particularly as hydrogen is considered to be a future clean fuel for both electrical power and vehicles [1-3]. Currently a few methods exist to produce hydrogen; methane partial oxidation ($CH_4 + 1/2O_2 \rightarrow CO + 2H_2$) [4], the water gas shift reaction ($CO + H_2O \rightarrow CO_2 + H_2$) [5, 6], steam reforming ($CH_4 + H_2O \rightarrow CO + 3H_2$) [7] or gasification of heavy carbonaceous materials.

These methods produce hydrogen mixed with undesired components such as CO and CO_2 and the reactions normally proceed at high temperatures and pressures. Among these methods, the most commercialized process for hydrogen production is the steam methane reforming (SMR) process in combination with water gas shift (WGS) reactors. Both of these processes yield thermodynamic equilibrium reactions which limit the removal of one product (particularly hydrogen). For such reversible reactions, using membranes for selective removal of hydrogen enables one to overcome equilibrium conversion [8, 9].

Separation and purification of hydrogen is a critical technology due to utilization of high purity hydrogen in electrical powered vehicles. Palladium-based membranes have emerged as an attractive technology to separate and purify hydrogen from the aforementioned methods because of their unique properties such as high permeance and theoretically infinite selectivity to hydrogen. However, stability and durability of membranes still remains a critical and technical challenge. Membrane production and operation costs need to be addressed for commercial applications. The movement aimed at promoting hydrogen as an energy carrier and reducing greenhouse and pollutant emissions produced by the consumption of hydrocarbon fuels is often referred to as the “hydrogen economy.”

To compete with the current fossil fuel economy, cost reductions are required throughout the different segments of the hydrogen economy, including hydrogen production and storage technologies [10]. Today membrane separation is one of the best available technologies for gas separation, although scientists are still trying to improve the membrane performance and reduce costs. Membranes are proving to be cost effective in replacing other purification and separation techniques. The expansion of membrane processes is in part dependent on the

development of membranes with improved performance fabricated from new materials. When compared with organic membranes for process application, much emphasis has been placed on inorganic membranes, including sufficient stability and high tolerance in the presence of organic solvents. Inorganic (ceramic) membranes have not been extensively used in the past due to a costly manufacturing process. With the development of phase inversion (spinning process), inorganic membranes could be obtained with smaller pores in a controlled manner. Spinning of membranes is a complex process that requires an understating of fabrication parameters that influence the properties of the membrane. In this regard, it would therefore be interesting to investigate these parameters in order to generate an understanding of the science involved, and later produce membranes with desirable properties.

1.1 Research objectives

Production of ceramic hollow fibre membrane as support for palladium membrane is the main aim of this research project. Additional aims of this research includes:

- To examine spinning parameters: air gap, bore fluid flow rate and extrusion pressure
- Production of YSZ support using phase inversion
- Formulation of dope solution with different water concentrations to investigate its effect on membrane performance, structure and rheological analysis
- To evaluate the effect of surface porosity and pore size on the support permeability
- To evaluate the effect of external coagulant fluid on the membrane structure and performance
- To investigate the influence of the suspension properties and the sintering conditions on the final support structure
- Characterize the obtained support in terms of pore size (mercury porosimetry), surface morphology (AFM), permeability and SEM

Chapter 2

2. Literature review

In the past few decades, membranes technology come into wide use in the petrochemical, electronics, pharmaceutical, food and beverage to environmental processes, such as waste water treatment [11]. Membrane technology has been applied commercially to separate individual components from mixtures of both liquids and gas [12]. Membrane separation is a technology which selectively separates (fractionates) materials via pores or minute gaps in the molecular arrangement of a continuous structure. During separation process, the goal is to allow purified components (hydrogen gas) to pass through the membrane freely, while hampering permeation of other undesired components [13].

Figure 2.1 illustrates the membrane process principle. A small fraction of the feed permeates through the membrane depending on the characteristics of the membrane. These characteristic include, selectivity, permeability and stability. The remaining fraction of the feed that contains particles rejected by the membrane is presented in the retentate, while the components which permeates freely through the membrane or at a high rate is presented in the permeate [13, 14]. This type of separation is driven by the pressure difference across the membrane.

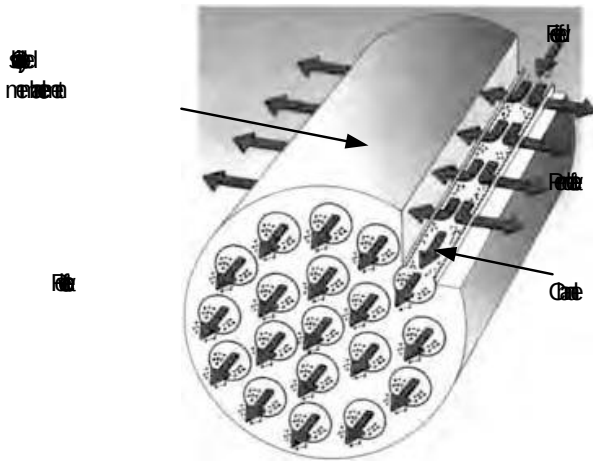

Figure 2. 1 Schematic representation of multichannel structure [15]

Common technologies employed for hydrogen separation include adsorption and desorption (pressure swing adsorption, temperature swing adsorption, electrical swing adsorption, and cryogenic recovery), selective condensation and membrane separation [2, 10, 16-20].

Membrane separation technology has received increased interest due to its simplicity, low energy consumption, low operating cost and ease of operation. Membrane technologies have economic potential of integrating hydrogen production and separation, while incorporating reaction and separation in the same unit [21]. These characteristics have directed much work towards the development for effective hydrogen membranes.

In practice, an important problem hindering the establishment of membrane processes as an alternative compared with other separation processes includes the lack of stable and selective membrane able to withstand harsh process conditions [22]. There are two types of synthetic membranes which are available for separation application; (1) organic membranes (polymeric) and (2) inorganic membranes (ceramic). Organic materials (polymeric membranes) have been prepared and used widely due to their high permselectivity and high surface area per unit volume [23, 24]. Many industrial separation processes require a membrane with a material that is not limited to mild operating conditions, ease of fouling as well as sufficient strength to endure aggressive environment for which organic membranes are unstable [25].

For this purpose inorganic membrane should be considered. Inorganic membranes, either porous or dense are made from materials such as metal, glass and ceramic (oxides) [26]. These materials are commonly used as support. Since porous membrane yield high permeance but low selectivity, while dense membranes have high selectivity and low permeance [27], composite inorganic membranes could be suitable to ensure both high permeance and selectivity at the same time. A support is typically porous and its main function is to yield mechanical support to a selective membrane layer. Composite membranes consists of a top layer/film deposited on a suitable porous material support [28, 29].

Layers/films made from metal elements which belong to group 10 and some metals in groups 3-5 of the periodic table have the ability to dissociate and dissolve hydrogen. From these metals, palladium (Pd) membranes have emerged as an attractive metal for separation and purification of hydrogen because of its unique superior properties such as high permeance, theoretically infinite hydrogen selectivity and showing high corrosion resistance in oxidation environments [16, 30-36]. Generally, the performance of Pd-based membranes can be evaluated in two terms: (i) permeability and (ii) selectivity. For high permeance of hydrogen, smaller membrane areas are desirable, resulting in lower material cost and higher productivity. For high selectivity of hydrogen, Pd based membranes require several tens of microns of palladium which lead to a decrease in hydrogen permeance and

costly production. The selectivity of hydrogen and permeability strongly depends on membrane properties, such properties will be highlighted in the section below. Pd-based membrane technology is so far the best technology for producing pure hydrogen [20, 37, 38]. Figure 2.2 depicts the operating principle of hydrogen separation.

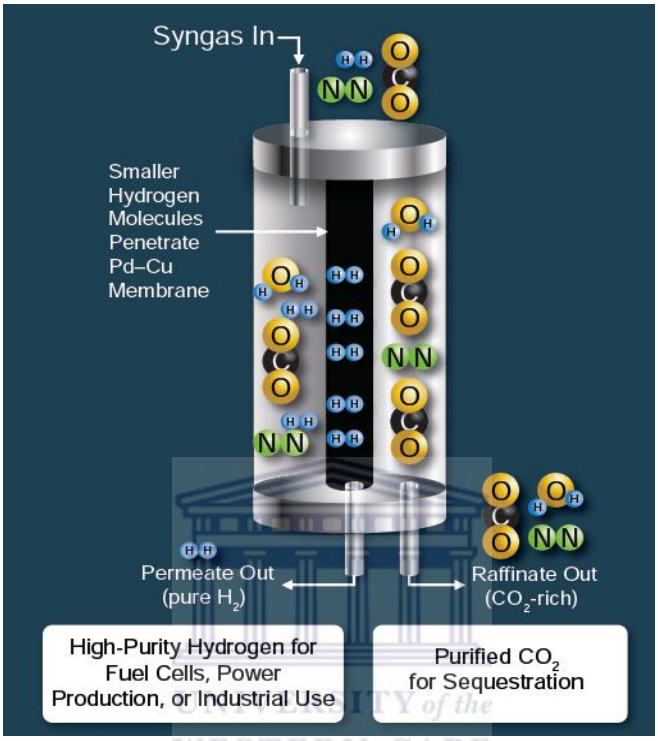

Figure 2. 2 Illustration of the operating principle of hydrogen separation [39]

2.1 Support for palladium based membrane

It was previously discussed that in order to obtain a successful high performance membrane, palladium has to be deposited onto a suitable support material, with appropriate chemical, thermal and mechanical strength. Regarding the types of materials used, supports for palladium based membranes reviewed in this section can be divided into three groups: glasses, metals and ceramics.

2.1.1 Porous vycor glass supports

Porous vycor glass supports (PVGS) are common substrates used in Pd-based composite membrane fabrication due to their smooth surface, relatively cheap and good thermal shock resistance. Drawbacks of using vycor glass supports are that they exhibit low permeance and they are mechanically fragile making their modularization a difficult challenge [40, 41]. In

addition, the relatively large differences in thermal, mechanical and chemical properties existing between the dielectric supports and metallic film (palladium) potentially create interfacial strains which may result in stress in the film. Porous Vycor glass substrates are not stable above 650 °C due to densification. Cuperus *et al.* [42] attempted to fabricate silica glass hollow fibre membrane for gas separation. They found that the membrane was too fragile to be used on a large scale.

2.1.2 Porous metal supports

Porous metal supports (PMS) can potentially be used as substrates for Pd-based membrane for various reasons; a) their thermal expansion coefficient is close to that of Pd-based membranes, b) their sufficient resistance to corrosion, c) good electrical conductivity based on electroplating of Palladium, d) their ease of being configured into various shapes with average pore size of 0.1-100µm and e) they can be sealed into a module more easily compared to ceramic supports [40, 43-45].

Among various metals studied, the most widely used support is porous stainless steel (PSS) due to its chemical resistance, ease of fabrication and low cost [29, 46, 47]. Commercially available stainless steel supports are often in form of disks or tubes with the smallest pore size of 0.2µm [48]. However, the surface of PSS support is generally rough [49], requiring a relative thick Pd layer (>10micron), as a consequence the hydrogen permeance through the composite membrane is typically not as high as desired. Pores on its surface are extensively larger than the ceramic alternatives, making it harder to produce a thin defect free Pd layer directly onto the PSS support [49]. For these reasons surface modification by abrading the surface, mechanically altering the surface, shrinking the pore size, sintering at high temperature and depositing other materials are sought to effectively reduce the roughness and the defects.

Materials such as ZrO_2, Al_2O_3, TIO_2, YSZ and CeO_2 are commonly used as barrier layers particularly when the selective layer and the support are metallic. These inter-metallic layers prevent the inter-diffusion between the PSS and the Pd layer and hence allow the entire membrane to be used in a methane steam reforming environment (at least 800 °C). Although surface modification is achieved, deposition of other materials onto the PSS support before Pd layer makes the production less economical.

According to Mardilovich [50] the Pd layer film thickness must be approximately three times as thick as the largest pore size diameter in order to obtain a leak-free membrane. Shu *et al.* [51] used 0.2µm porous stainless steel and found a dense and defect free film by depositing at least 15µm of metal using an electroless plating (ELP) method. Jemaa *et al*. [52] prepared Pd membranes supported on porous stainless steel disks using the ELP technique. They modified the surface of stainless steel support with 5-6µm pore size opening by shot peening treatment with iron. They claimed that the original pore openings were reduced to approximately 1µm after 300s treatment.

2.1.3 Porous ceramic supports

Porous ceramic supports (PCS) are a broad class of non-metallic substrates which provides a structure that gives high hydrogen flux at a low cost. The combination of high thermal, chemical and mechanical stability, easy fabrication, low fouling rate, long and reliable service life, sufficient strength to sustain expansion and contraction of lattice with varying hydrogen concentrations, high surface area/volume ratio, controllable pore size (5-200nm) and high operating conditions [11, 12, 20, 26, 53-59] has made ceramics an interesting alternative substrate for palladium membrane where metals suffer from limited stability.

Ceramic supports can be categorized on the basis of its structure: symmetric and asymmetric. Figure 2.3 illustrate various structures of applicable synthetic membranes [60]. Symmetric membrane can be porous, cylindrical porous and homogenous (non-porous). Porous membranes usually have an interconnected and torturous (like sponge) structure [61] whereas dense membranes hold no pores of microscopic dimensions. This implies that all unoccupied volume is free space between the segments of the macromolecular chains [62]. Asymmetric membranes are typically porous and are comprised of various layers with different pore size distribution [63, 64].

Ceramic asymmetric membranes generally have a macro-porous support providing the mechanical strength, one or two intermediate meso-porous layer(s) with the role to reduce any inherent defects of the support and the top micro-porous/dense layer which provides the system with its selective properties [58, 63, 65, 66]. The graded system of asymmetric supports formed by adding one or more intermediate layers with gradually decreasing thickness and pore size makes it feasible to deposit defect-free thin Pd films [67, 68]. Asymmetric supports are good substrates for Pd membranes because of their low gas flow resistance and smooth surface, readily suitable to accept a thin film. Additional features of a

suitable homogeneous surface support include a narrow pore size distribution and a particle size range smaller than the Pd layer thickness [40].

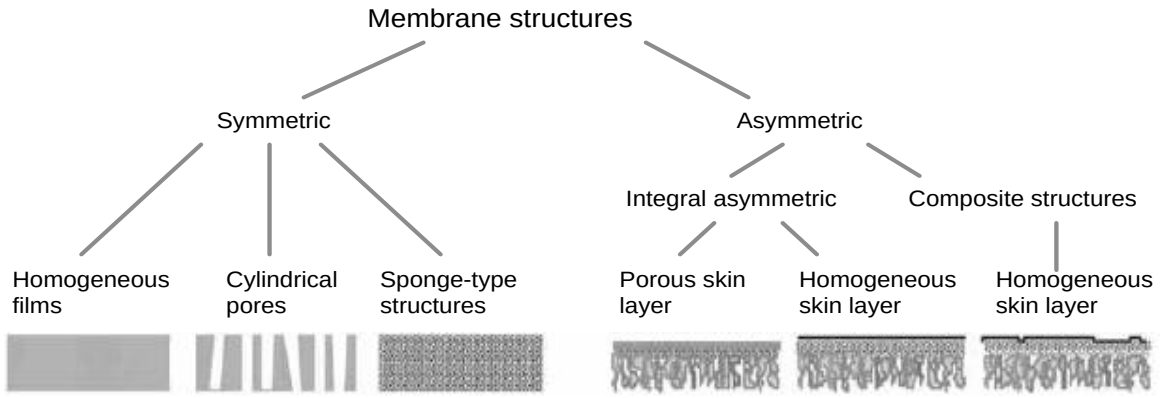

Figure 2. 3 Schematic illustrating various structures of applicable synthetic membranes [60]

Preparations of ceramic supports have been improved over the last decade, however the commercially available ones are still limited to four oxides namely; silica, zirconia, titania and alumina [13, 63, 69]. Currently, commercially available ceramic supports are in a form of tubes and hollow fibres. However, due to their brittle characteristics they should be handled with greater care than metal supports [40]. Despite the fact that a high radius of curvature impairs the durability of ceramic composite materials when undertaking sustained high temperature cycling, small radii hollow fibres products are still one of the most promising substrate. The large packing density and potential low manufacturing cost of hollow fibre substrates outweigh advantages of other substrates, especially when considered for compact hydrogen production systems in mobile fuel cell units [16].

Luiten-Olieman and co-workers [70] recently developed both ceramics and metallic hollow fibre supports as a way of increasing the surface area to volume ratio. According to Pan *et al.* [71] ceramic hollow fibre provide supports with packing density as high as $1000 m^2/m^3$. Okazaki *et al*. [72] studied the effect of ceramic support on the flux of hydrogen at high temperature. They reported that at temperatures higher than 650 °C, alumina reacts with hydrogen and the Pd-Al alloy formed decreases the permeation of hydrogen to a point where no permeation occurs, for example at 850 °C whilst YSZ is more stable and can be used to temperatures as high as 750 °C. SiO_2 supports are well known for significantly longer service-life.

A major limitation in the use of SiO_2 as supports for Pd based membrane is that they can only withstand the temperature up to 300 °C without degradation of the membrane material [73], making it harder to use the entire membrane in a steam reforming environment. TiO_2 supports have been reported to have better antifouling abilities [69] and enough rigidity. In comparison with other ceramic supports, yttria-stabilized zirconia (YSZ) is more preferable due to the following reasons: (i) it has superior chemical strength; (ii) it is relatively inexpensive; (iii) it exhibits high oxygen ion transfer number and great mechanical stability at elevated temperatures such as those used in steam reforming of methane due to better stability of ZrO_2 materials [63, 67, 68, 74, 75]. Also YSZ can be used in liquid filtration with much better alkali durability than other ceramic membranes [57].

2.2 Palladium based membranes

2.2.1 Unsupported Pd membranes

Commercially available unsupported Pd membranes are typically thick (>50 µm thick) in order to meet the minimum mechanical stability requirements [53, 76, 77]. However, various critical challenges still limit commercial applications of Pd-based membranes. For instance, Pd membranes are excessively costly, implying that the cost of the whole membrane will increase considerably with increasing membrane thickness. Subsequent to that, these membranes yield lower hydrogen permeation i.e. lower productivity. Other challenging problems of Pd membranes are the embrittlement resulting from hydride phase transition and the susceptibility of separation membranes to fouling by common contaminants found in syngas such as sulphur and carbon monoxide gases. In order to improve these important aspects much effort has been expended in achieving higher hydrogen permeation while lowering the cost of Pd membrane [16]. Interestingly, the key to success in this regard is to produce a high quality support material for palladium membranes.

2.2.2 Supported membranes

A supported/composite membrane consists of a porous support (particularly ceramic or metal) which provides the mechanical strength and a thin top layer (palladium) synthesized onto the support [28, 29]. On the other hand, the quality of the support surface is crucial to the integrity and the thickness of the top Pd layer. Particularly when the thin film membranes are selected, supports that have much lower pore size and smoother surface area are

desirable. Thinner Pd films commonly provide a structure which yields higher hydrogen permeance, well higher than the unsupported membranes, better mechanical properties, good stability, and low material costs without compromising the selectivity [28, 33, 76, 78]. The final quality membrane depends on the deposition technique and the support material.

Considering methane as one of the most accessible fuel of the future, a steam methane reformer integrated with a palladium membrane is desirable, implying that the future thin composite palladium membranes in the reformer must be characterized by long stability under harsh operating environments such as high temperature and pressure. The main focus of the current research work is to develop a cost effective Pd-based membrane that will be able to operate in methane reforming process environment. While other researchers in the department are working on optimization of the Pd film production, this thesis work has been dedicated to develop the most suitable and cost effective YSZ support structure for Pd-based composite membranes that will be able to withstand high temperatures and harsh chemical environments. The support of choice has been selected based on the literature review.

2.3 Fabrication processes of ceramic supports and membranes

There are different methods that have been developed to synthesize ceramic support. Preparation steps involve: (1) formation of particle suspensions; (2) packing of the particles in the suspensions into a membrane precursor with a certain configuration (flat or tube precursor) and (3) consolidation of the precursor through sintering at high temperature [1, 13, 66]. A simplified flow diagram for preparation of asymmetric/symmetric supports is displayed in Fig 2.4. Methods such as slip casting, tape casting, extrusion and pressing are proved to be the influential techniques which turns the paste or slurry into a green fibre or precursor [1, 13, 66]. Further illustration on the production of composite membranes through a coating step using either dip-coating, sol-gel, chemical vapour deposition (CVD), ELP process followed by a sintering step is shown in Fig 2.4.

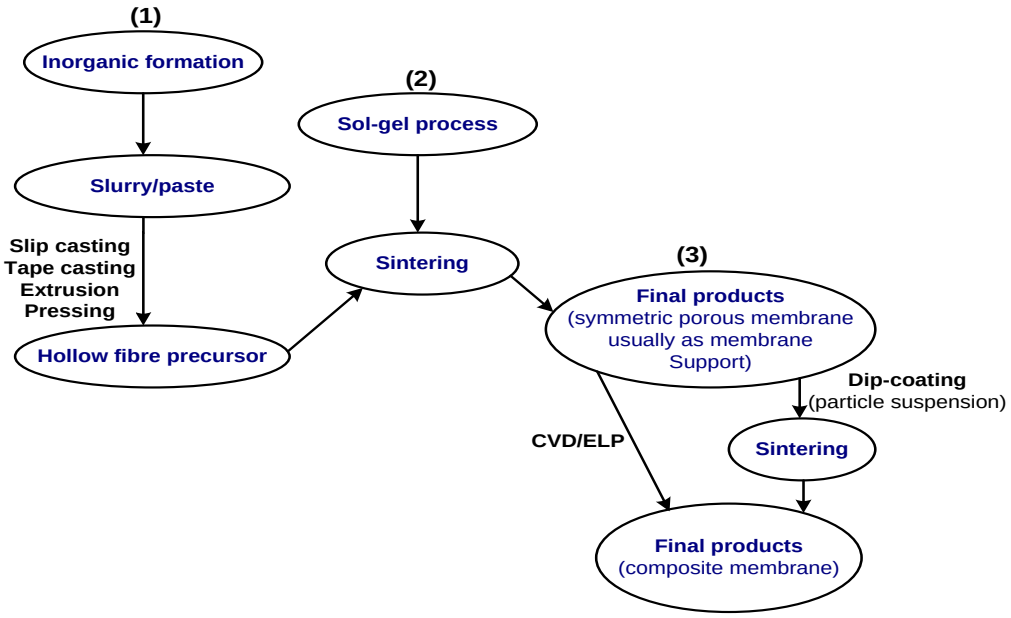

Figure 2. 4 A simplified flow sheet for preparation of ceramic membrane using various conventional methods [1]

2.3.1 Slip casting method

Slip casting is one of the methods of obtaining a ceramic membrane or support. The principle is as follows. A well-mixed powder suspension is poured into a porous mould, where the capillary suction forces the solvent of the suspension to be extracted into the pores of the mould to form a gel layer. Gelation must occur fast to avoid penetration of the suspension of particles into the pores of the mould. Leenaars and Burggraaf [79] and Uhlhorn *et al.* [80] investigated some of the processing parameters such as solid concentration, particles diameter and viscosity of the suspension. Tiller and Tsai [81] reported a theoretical modeling of the slip casting process. The slip casting method is generally used to produce ceramic products with a relative thick wall. Pottery, toilets and basins are typically produced using slip casting. Casting times are relatively long, and Figure 2.5 shows a schematic overview of a typical slip casting process. Slip casting can be used to produce tubular objects but not commonly used to produce thin walled items.

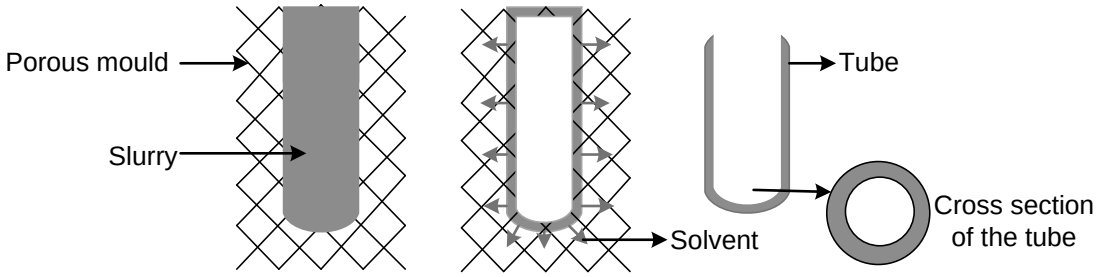

Figure 2. 5 Slip casting illustration [1]

2.3.2 Tape casting method

Tape casting is a method used to produce flat sheet ceramic products. In this method, the cast is set in motion once the powder suspension has been poured into a reservoir behind the casting knife as shown in Fig 2.6 [1, 82]. The thickness of the cast layer is determined by the gap between the knife blade and carrier. The solvent is evaporated from the surface immediately after the wet cast layer has passed the drying chamber giving a dry membrane precursor on the carrier surface. The membranes prepared with this method typically range from 250-1250µm. Gestel *et al*. [22] prepared PSS support with a thickness of 0.5µm for the development of hybrid metallic-ceramic membranes. The obtained support had continuous surface layers with the pore size of 650nm.

Boaro *et al*. [83] synthesized YSZ membranes by tape casting method using both pyrolyzable pore formers and NiO followed by acid leaching. It was shown that the porosity of YSZ wafers increases in a regular manner with the mass of graphite to between 60-75% porosity. It was observed, from cross sectional scanning electron microscopy (SEM) analysis, the shape of the pores in the final ceramic were related to the shape of the pore formers, implying that the pore size of YSZ wafers can be controlled by choice of pore former. Tape casting can be used to produce thin ceramic products with controllable pore size. However, the product's shape is typically flat. Since the ceramic slurry needs time to set, the production of tubular product (produced in vertical direction) is more challenging.

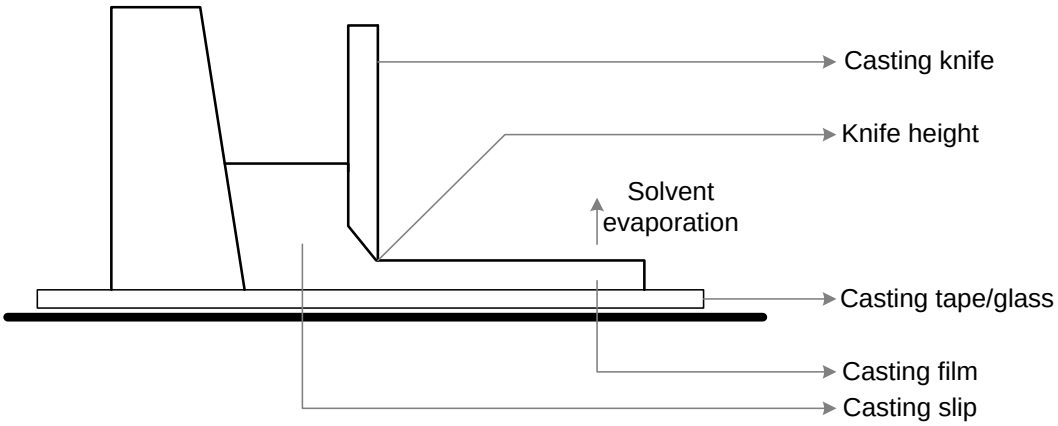

Figure 2. 6 Tape casting [1]

2.3.3 Pressing method

The pressing method shown in Fig 2.7 is used in the production of disc shaped inorganic products. Usually the machine is used to apply pressure to press powders into a compact disc. The force exerted on the machine joins the particles together and hence forms a compact layer. The thickness of ceramic membranes prepared with this method is approximately 500µm [1, 82]. In previous study Xia and Liu [84] prepared Gd-doped ceria (GDC, $Gd_{0.1}Ce_{0.9}O_{1.95}$) electrolyte products using the pressing method.

A highly porous structure with pore size ranges from tens of nanometers to several micrometers was observed. Their membrane thickness was 8µm. They studied the GDC membrane in a solid-oxide fuel cell with air as oxidant and humidified hydrogen. The permeance of the membrane to molecular gases showed significant results due to the open circuit voltage of about 1V. While the pressing method is typically used for the production of flat substrates, one sided tubular shapes can also be produced. As a mould is required for each item to be produced, product with small diameter will become relatively expensive and the pressing method is usually not considered for tubular supports with small radii (<10mm).

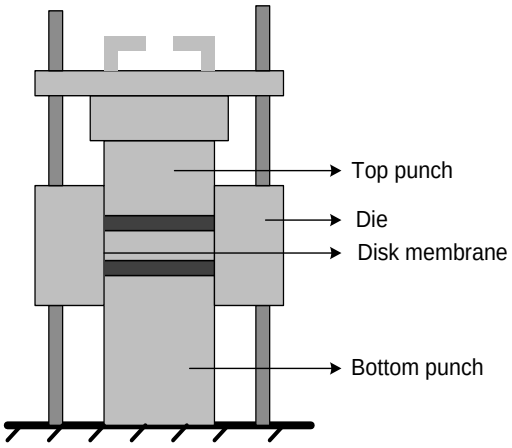

Figure 2. 7 Pressing method [1]

2.3.4 Extrusion method

The extrusion method is commonly used to produce construction material such as brick and tile, furnace tubes, heat exchanger tubes, magnetic and electronic substrates and ceramic tubular support. It has hardly any limitation in terms of product length; it can produce large products ranging up to 1 ton and small products with mass a few grams [1]. The extrusion process produces a homogeneous (symmetric) product. Membrane applications from extruded tubes are mostly found in the water purification industry. Figure 2.8 illustrate the extrusion process.

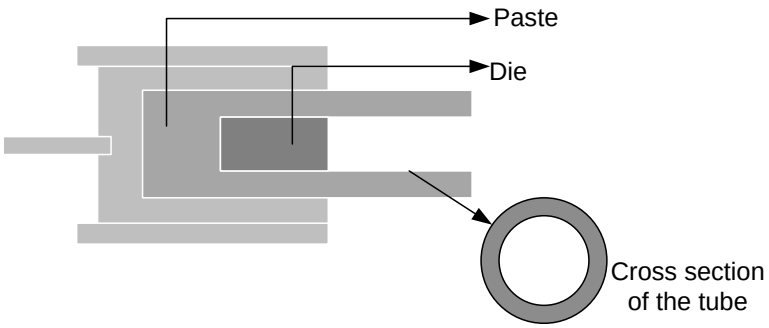

Figure 2. 8 Extrusion illustration [1]

2.3.5 Sol-Gel process

Ceramic membranes had little application in the past before the development of sol-gel process. In the late 1960's, much interest was shown in ceramic industries, mostly because ceramic composite membranes could be obtained with smaller pores with the development of sol-gel [1, 13, 22]. This method forms a network of partially hydrolyzed and poly-

condensed monomers diluted in a solvent. A porous structure is prepared by applying a coating layer, drying and calcinations [1, 13]. A drawback of this process is that it involves strong acids and other toxic substances. As shown in Fig 2.9 sol-gel method is categorized into two processes and they are further discussed in the subsequent section.

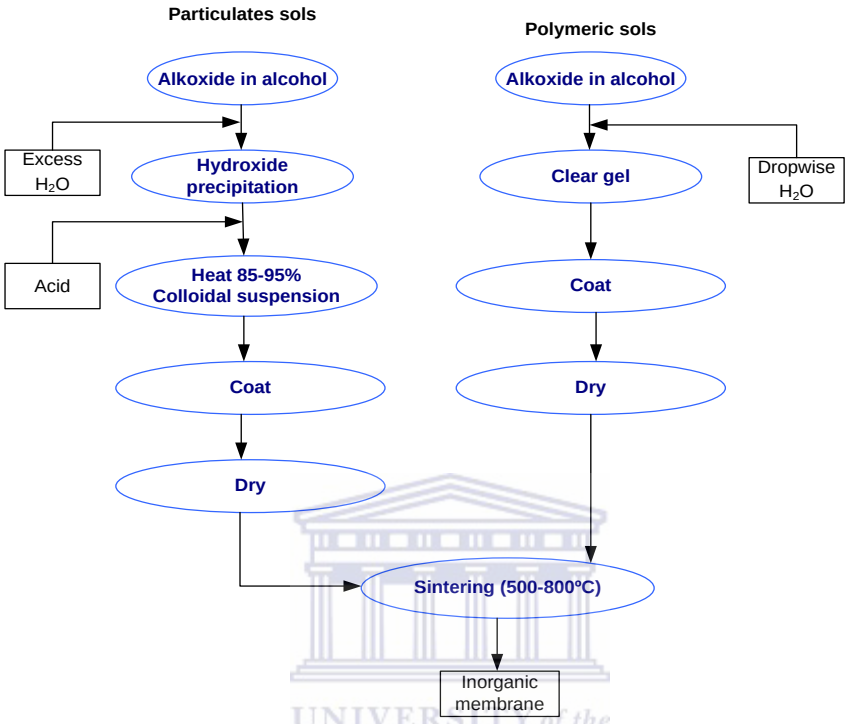

Figure 2. 9 Sol gel process [13]

2.3.5.1 Particulate sol-gel process

In the particulate sol-gel process, a metal alkoxide dissolved in alcohol is hydrolyzed by adding excess water or acid, followed by a process called peptization whereby the precipitate produced is kept as a hot solution for a long period of time which eventually forms a stable colloidal solution. Then, the colloidal solution is cooled, coated onto the micro-porous support membrane and finally calcined at 500-800 °C. The reactions involved are as follows: [1, 13].

Precipitation: $Al(OR)_3 + H_2O \rightarrow Al(OH)_3$

Peptization: $Al(OH)_3 \rightarrow \gamma - Al_2O_3 \cdot H_2O$ (Böhmite) or $\sigma - Al_2O_3 \cdot 3H_2O$ (Bayerite)

Calcination: $\gamma - Al_2O_3 \cdot H_2O \rightarrow \gamma - Al_2O_3 + H_2O$

2.3.5.2 Polymeric sol-gel process

A metal alkoxide dissolved in alcohol is obtained by adding a certain amount of water into the solution which stimulates a reaction of an active hydroxyl group on the alkoxide. Then, the formed inorganic polymer molecule is coated onto the ceramic support, dried and sintered to form a metal oxide film. The equations, shown below, depicts the overall process [1, 13].

Hydrolysis: $Ti(OR)_4 + H_2O \rightarrow Ti(OH)_2(OH)_2 + ROH$

Polymerization: $nTi(OR)_2(OH)_2 \rightarrow [Ti(OR)_2 - O]n + H_2O$

Crosslinking: $[Ti(OR)_2 - O]n \rightarrow [Ti(OH)_2 - O][Ti(OH) -)O]$

A nano-composite membrane of polyacrylonitrile (PAN) with hydrolysate of tetraethoxysilane (TEOS) as the inorganic phase showed a good performance in O_2/N_2 separation, as was observed by Iwata *et al*. [85]. Buckley and Greenblatt [86] investigated the pore characteristics of xerogels prepared with TEOS, ethanol and water. They found that by increasing the ethanol content of the solution, the particle size decreased. They also reported that increasing the alkyl chain of the alcohol solvent, the xerogel structure changed from micro-porous to meso-porous. Finally, they showed that high water content favoured macro-porosity, while low water content favoured meso-porosity. Baker *et al*. [87] investigated organic oligomers and surfactants as possible modifying agents for xerogel. They stated that the incorporation of organic components within sol-gel process leads to composite that can help to produce crack free materials and improve coating substrate adhesion.

2.3.6 Dry-wet spinning

Since the initial studies of polymeric hollow fibre membrane by Loeb and Sourirajan [13], many patents and technical papers have reported different techniques to synthesise ceramic fibre membranes. The spinning process is very similar to the extrusion process, however, there are a few differences between them. In an extrusion process (Fig 2.6), a paste comprising of polymers, ceramic fillers, binders is compressed and forced through a nozzle. The precursor formed should at least show plastic behavior, because at lower stresses it behaves like a rigid solid and would deform when the stress reaches the yield stress [82]. In the spinning process, a suspension is compressed and configured into a tubular precursor in

a coagulation bath via a spinneret [88]. The precursor formed using spinning exhibits asymmetric/symmetric structure while it possesses a homogenous structure if prepared through extrusion.

The various methods favour either the production of a tubular or a flat product. As described in the previous section, ceramic supports were recommended to handle the harsh methane steam reforming environment at temperatures up to 850 °C. The shape of the ceramic support is also an important parameter. A flat area has to be sealed at all four sides. A tube has to be sealed at 2 sides but a one sided tube only requires one side to be sealed. Since sealing solutions compatible between ceramic at the one end and the metal from the reactors end in an environment that cycle between 0-850 °C is challenging, tubular supports are preferred. Dry-wet spinning process produces tubular configuration and this is elaborated further in the subsequent hollow fibre synthesis.

2.4 Preparation of hollow fibre ceramic membranes using dry-wet spinning

The preparation of inorganic hollow fibre membranes has been established for several decades [25, 89, 90]. It is achieved through multi-step process and a combination of various methods [63, 91]. As illustrated in Figure 2.10, a support layer of porous substrate is prepared to provide a membrane with mechanical strength, followed by coating intermediate layers on the support layer prior to fabrication of the final separation layer [26, 57]. The multi-step process described above has been used to prepare most ceramic asymmetric/composite membranes. Studies shows that this type of process is too complicated, hence time and energy consuming which requires several expensive heat treatments leading to high cost of inorganic membranes [26, 63].

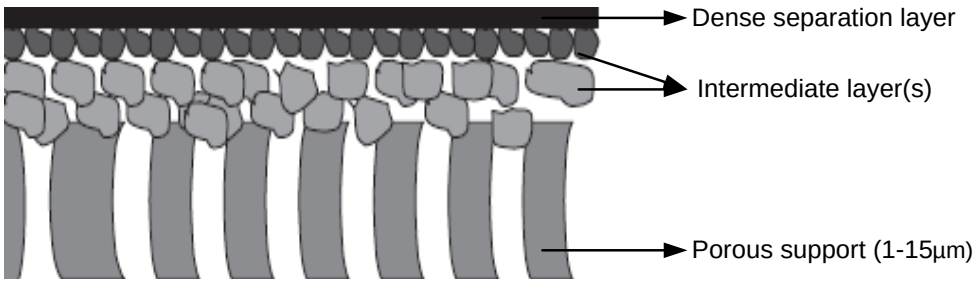

Figure 2. 10 A general structure of ceramic membranes [91]

High membrane cost drove membrane technologist and researchers to combine multiple steps into a single step as a way of lowering production cost. Most research and development show that fabrication of inorganic hollow fibre follows similar procedures but uses substrates in hollow fibre geometry. Tan *et al.* [12] and Liu *et al.* [92-94] successfully produced hollow fibre ceramic membranes using phase inversion which involves three steps namely: (1) preparation of a spinning suspension; (2) spinning of ceramic hollow fibre precursors and (3) a sintering process. A detailed discussion of these three steps (Fig 2.11) follows and includes: (1) factors that affect the structural morphology of a membrane including particles size and rheology; (2) mechanism of phase inversion and (3) sintering process.

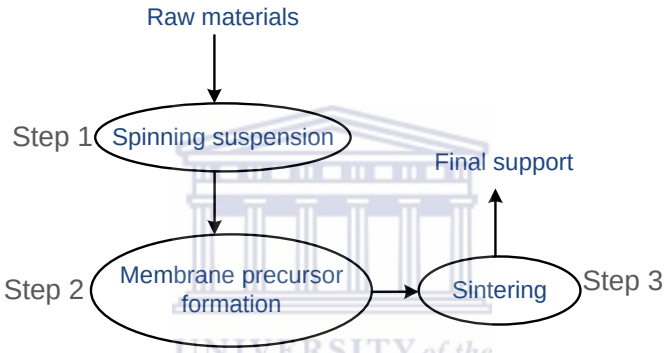

Figure 2. 11 A three step procedure for preparation of hollow fibre ceramic membranes [26]

2.4.1 Preparation of spinning suspension

The preparation of the spinning suspension involves mixing a dispersant and solvent of choice, adding particles, polymer binders/plasticizers for dispersion and degassing the suspension prior to spinning [1]. The dispersion step is one of the most important steps as agglomeration of the particles in the spinning mixture would have an effect on the quality of the final product [95]. In selection of spinning suspension particularly ceramic powder, the particle sizes and their distribution have an effect on the porosity, pore size and pore size distribution of the final product. The process for obtaining and holding the powder particles in a hollow fibre configuration relies on the other components in the spinning suspension because they predesign the membrane morphology [1]. One of the biggest issues encountered by membrane technologist is the formation of agglomerates during synthesis. The ceramic powders being added into the spinning suspension are typically in a form of soft agglomerates which have a tendency to trap air in the interstitial space between the particles [1].

Agglomeration causes bumpy distribution of particles in the membrane, resulting in pin holes and unwanted surface porosity in the final membrane. If the soft agglomerates are not broken up when the polymer binder is introduced into the suspension mixture, the binder will automatically cover the soft agglomerates instead of covering the individual particles. The latter is a result of permanent group of soft agglomerates that occurs throughout the entire process, which in turn will hinder high shrinkage during the sintering process [1]. Weakly agglomerated nano-crystalline powders can be obtained by routinely using mechanical modification which involves the use of mixers [96] or sonicators in order to physically disperse the particles through the shear force[97], and chemical modification which involves the use of surface pre-treatment.

Luiten-Olieman *et al.* [70] controlled the size of YSZ and Al_2O_3 nanoparticles within the PES matrix by utilizing ultrasonic bath. The benefit of dispersion is to break apart any soft agglomerates and keep the particles apart by steric effects. Once the dispersion step is complete, binders and additives are added into the suspension and the mixture is stirred to avoid clumps. Addition of additives results in an increase in the solution viscosity, which increases with an increase in the additive molecular mass. A final step in spinning suspension procedure is degassing. After the spinning suspension has been mixed and degassed, it is ready for spinning as described in the next section.

2.4.2 Spinning of ceramic hollow fibre precursor

The spinning process is where the precursor or green fibres are spun through a spinneret. The nitrogen pressure is typically used to control the extrusion rate. De-ionised water or tap water is used as the internal and external coagulants. The spinneret allows the precursor to be extruded vertically downwards into the external coagulation bath. This is followed by washing and drying [1]. “Triple orifice” is one of the most widely used spinnerets because it allows much better control of the conditions applicable for spinning various types of hollow fibre. Two polymer dopes can be injected simultaneously, one dope in the outer orifice and the other in the inner orifice. The internal coagulant must be injected into the inner tube at the same time as the commencement of spinning.

During the spinning process, the outer dope is first exposed to air and vapor of the coagulation bath and then to the external coagulant, while the inner dope is in contact with the internal coagulant. The internal coagulant is utilized to form the inner layer, while the external coagulant is utilized to form the outer layer [98]. Spinning parameters such as the

air gap, internal coagulant, pressure and the solvent used for both internal and external coagulation highly affect the morphology of ceramic membrane. The use of triple orifice spinnerets makes it easy to control such spinning parameters. De Jong *et al.* [99] attempted to use a triple orifice spinneret to spin two particles suspension containing different sized Al_2O_3 particles simultaneously. Li *et al*. [100] previously used triple-orifice spinneret to control the external coagulation rate of the hollow fibre, where the first external coagulant was extruded from the outer orifice [98]. The process in which the precursor is formed into a hollow fibre configuration is presented in the following subsection.

2.4.2.1 Phase inversion

Asymmetric/composite hollow fibre membrane may be prepared by dry/wet technique which is based on the principle of phase inversion [100]. With this technique, any type of membrane morphology can be obtained since many parameters involved can be varied [63, 99]. Phase inversion can be described as a process whereby a polymer solution of two or more components is converted into two phase gel: solid (polymer rich) phase and liquid (polymer poor) phase. In general, the formation of membrane by phase inversion can be described in terms of three component system: non-solvent, solvent and polymer [1, 63, 101].

Phase separation in the polymer film is caused by an exchange of solvent and non-solvent [24] which leads to the thermodynamic instability of the spinning suspension and induced liquid-liquid de-mixing. Solidification of the polymer rich phase is stimulated by additional exchange of the solvents and non-solvents [13]. Between the spinneret and non-solvent bath there is an air gap where the membrane formation starts, which can lead to a variety of characteristics asymmetric or symmetric structures [63, 100, 102]. A complex three component phase diagram used in the membrane preparation is shown in Fig 2.12. The diagram consists of two regions: (1) a region which is characterized by miscible components, the one phase region; (2) and a region where-by systems separates into solid (polymer rich) phase and a liquid (polymer poor) phase, the two phase region [13].

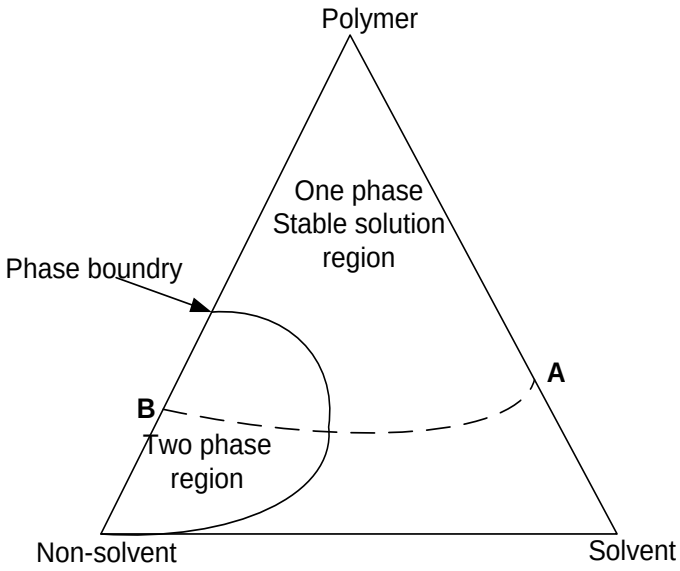

Figure 2. 12 Schematic representation of a phase diagram for ternary system [13]

Compositions A represent the spinning mixture. During the spinning process the configuration changes to B, which aggregates to two separated phases. Systems with a high rate of phase inversion form macro-voids with fingerlike structures, for example (Fig 2.13b), whilst systems with a slow rate of phase inversion form sponge-like structures, for example (Fig 2.13a) [103].

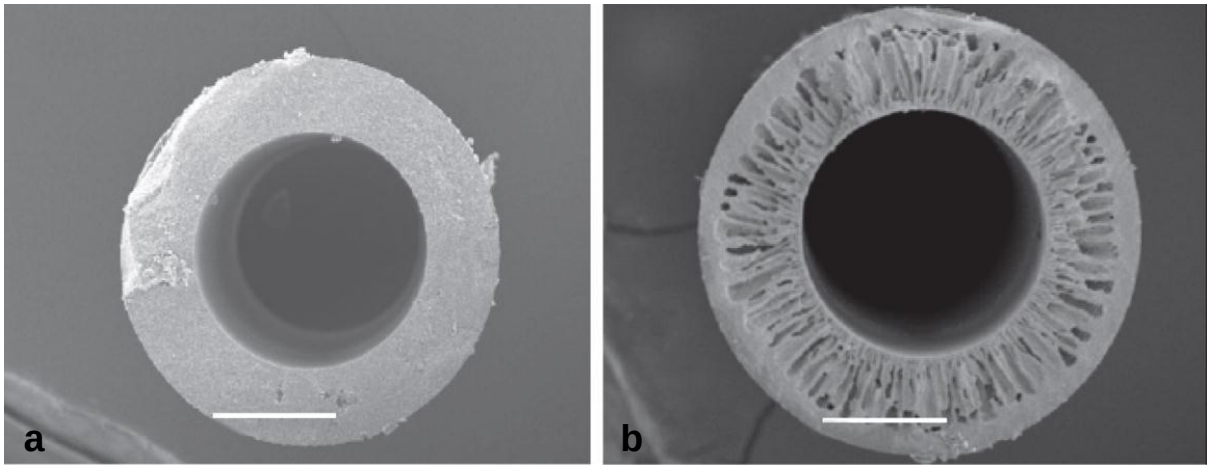

Figure 2. 13 Structure of the inorganic hollow fibre membranes: (a) symmetric, (b) asymmetric [26]

2.4.2.2 Factors affecting the spinning process of hollow fibre

Many parameters are involved in the phase inversion technique and these interact during extrusion or coagulation steps [104]. The dope solution is directly affected by the composition and selection of material (concentration, solvent, additive). The material must have good mechanical properties, it must be spinnable into a hollow fibre and it must be incorporated into the phase inversion technique. This principle is typically the starting point of the selection process. Other related parameters that affect the morphology of the hollow fibre membrane and its performance include: dope viscosity, composition of coagulants (interior and exterior), air gap, air moisture, bore fluid pumping rate and dope extrusion rate.

The viscosity of the spinning suspension is one of the most important parameter in the course of manufacturing hollow fibre membranes. The rheological properties play a key role in controlling the shape forming behaviour of a final precursor [105]. This topic has been widely studied. According to Li [1] a high viscosity is necessary to prevent the drawn fibre from breaking up into droplets. Benjamin and Kingsbury [56] investigated the viscosity of spinning mixture by using water as an additive. They found that the viscosity of the spinning suspension increases with increasing water concentration. Similar observation was made by Luiten-Olieman *et al.* [106]. They also observed that spinning suspension with higher particle loading exhibit higher viscosity.

The composition of the coagulants and rate of its delivery significantly influence the membrane morphology and performance. Zhang *et al*. [57] prepared YSZ hollow fibre membrane using ethanol as the external coagulant. Their cross sectional structure showed an asymmetric structure with an outer skin layer and highly porous sub-layer composed of long and large finger-like pores, whereas YSZ hollow fibre membranes prepared using water as the external coagulant shows thick sponge-like structures sandwiched with short and small finger-like structures near the outer and inner walls. Finally, they showed that the YSZ hollow fibre membranes prepared using ethanol as the external coagulant exhibited much higher water permeation than these prepared by using water as the external coagulant because of low fluid resistance.

The effects of air gap length on the hollow fibre membrane have been investigated by many researchers, and the effect on the morphology of the hollow fibre membrane and permeation properties reported often provide conflicting observations. For example, Aptel *et al*. [107] studied the effect of air gap on the membrane morphology of polysulfone hollow fibre membranes. They noted that permeability decreased as the length of the air gap increased.

The air gap length had no effect on the permselection properties of polysulfone hollow fibre membranes, as observed by East *et al*. [108]. Liu *et al*. [109] observed that the permeability of polyethersulfone hollow fibre membranes decreased with an increase in the length from 30-200cm. The effect of air humidity was revealed by Cluasi *et al*. [110]. It was determined that neither the presence of volatile solvent in the spinning suspension nor absorption of water from air gap were necessary to form nearly defect free membranes. The composition of bore fluid and its flow rate determines the formation of precursors, however the pressure within the nascent bore determines the initial filament diameter [104].

2.4.3 Sintering

Sintering is a process which enable the removal of organic components, bond the inorganic particles into a fibre product and hence retain the morphology of the hollow fibre membrane [92]. The spontaneous strengthening of green fibres by the effect of elevated temperature involves shrinking and densification. Sintering is the last step in the production of porous ceramic support for the application of membrane technology. Strengthening via sintering is essential but a decrease in the permeability is not desirable. Grain growth, a decrease in porosity, change in pore shape and increase in neck area occurs at this stage [1]. At the beginning, the particles have one point of contact from which an expanded neck is formed. Once the neck is formed, the particles enfold a spherical pore that tends to contract by the effect of the surface tension.

At this point the particles are most likely to deform. If particles allow for deformation, the pores will contract until the pressure of the gases trapped inside the pore is equal to the contracting force of surface tension. From this point forward, the pore will continue to contract at a higher or lower rate depending on the rate at which the gases are released from the pores through diffusion. Figure 2.14 illustrate the sintering process. The effect of sintering temperature has been studied but the results obtained by various scientists vary. Lin *et al.* [111] found the pore size of the alumina membrane to increase sharply at a temperature around 900 °C. Leavanen *et al*. [112] found that both the pore size and water permeance increases with increasing sintering temperature. Wei *et al*. [63] investigated the effect of particle size on the properties of the support. They found that smaller particle size enhances densification of the membrane. Wang *et al*. [113] found that the pore size of the supports increased with increasing temperature, whilst the pore size distribution remained constant.

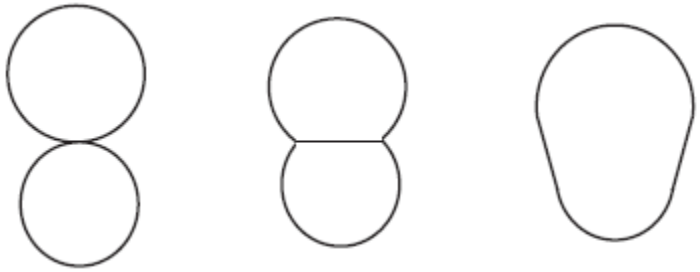

Figure 2. 14 Sintering process [1]

2.5 Overall concluding remarks

Metal supports offer advantages such as high mechanical strength, resistance to corrosion and their thermal expansion coefficient is close to that of Pd-based membranes, but they have drawbacks such as a rough surface and larger pore sizes. Ceramic supports offer advantages specifically when intended for application as a support for Pd based membranes in a methane steam reforming environment and thus being the focus of this study. Fabrication processes such as tape casting and sol-gel are believed to be less suitable to produce ceramic supports in a tubular configuration. In general, phase inversion provides control over the morphology

To this date, the phase inversion approach is the most widely used technology to produce ceramic hollow support at a lower cost than the methods currently utilized in the ceramic industry. A well-designed phase inversion/sintering process coupled with an optimal spinning suspension and parameters is the key in obtaining asymmetric/symmetric hollow fibre membranes with desired permeation characteristics as well as excellent strength. This research project covers immersion induced phase inversion because of its unique operations. It is a versatile technique which permits a wide range of morphologies from porous to non-porous/dense structure.

Chapter 3

3. Experimental results

A two-step membrane synthesis method has been used for the experiments in this work. This experimental section is divided into two sections: (i) deals with the materials used for synthesis of ceramic hollow fibre membrane and (ii) the experimental procedure followed for the synthesis of the membrane.

3.1 Materials

8 mol% yttria-stabilised zirconia powder (YSZ8-TC, particle size 0.5-0.7µm, surface area 6.7m^2/g) was used as the material support and it was purchased from Fuel Cell Materials (US). Polyethersulfone (PES, Ultrason, E6020, Perlen, Germany) and N-methylpyrrolidone (NMP, HPLC grade, Industrial Analytical, South Africa) were used as the polymer binder and solvent, respectively. Polyvinylpyrrolidone (PVP K85-95, Across Organics-US) was used as an additive. Tap water was used as external coagulant. De-ionised water and NMP were used as internal coagulant. Liquid nitrogen was used to break green fibres (Linsol, Cape Town). Pattex glue was used to seal one end of the hollow fibre (Pick n Pay, Cape Town).

3.2 Membrane synthesis

The membrane synthesis methodology adopted will follow a four-step synthesis whereby the polymer solution will be subjected to (1) the spinning step, (2) extrusion, (3) coagulation and (4) sintering

3.2.1 Preparation of spinning suspensions

Preparation of a spinning suspension may consist of a number of steps: (1) mixing particles of choice and a solvent; (2) adding polymer binders and additives and (3) degassing the suspension prior to the extrusion step. In this study, yttria-stabilised zirconia powder was selected as a material of choice due to its characteristics over ceramic powders. YSZ (31,7-55 wt%) was added to a mixture of N-methylpyrrolidone and water (0-5 wt%). The mixture was ultrasonically treated for 15minutes to break down YSZ agglomerates, while CAT R100C was used at a speed of ~100 rpm to ensure a uniform dispersion (Fig 3.1, step 1).

Subsequently, polyethersulfone (PESf) was slowly added in three steps, separated by 2 hours and the spinning suspension was stirred overnight. Polyvinylpyrrolidone (0-1 wt%) was added to modulate the viscosity of the spinning suspension, followed by stirring overnight. The viscosity of the spinning suspension was taken prior to degassing. Afterwards the spinning suspension was degassed at room temperature by applying vacuum for 2 hours and left overnight under dry air (Fig 3.3 step 2A). The composition of the used spinning suspension is specified in Table 3.2.

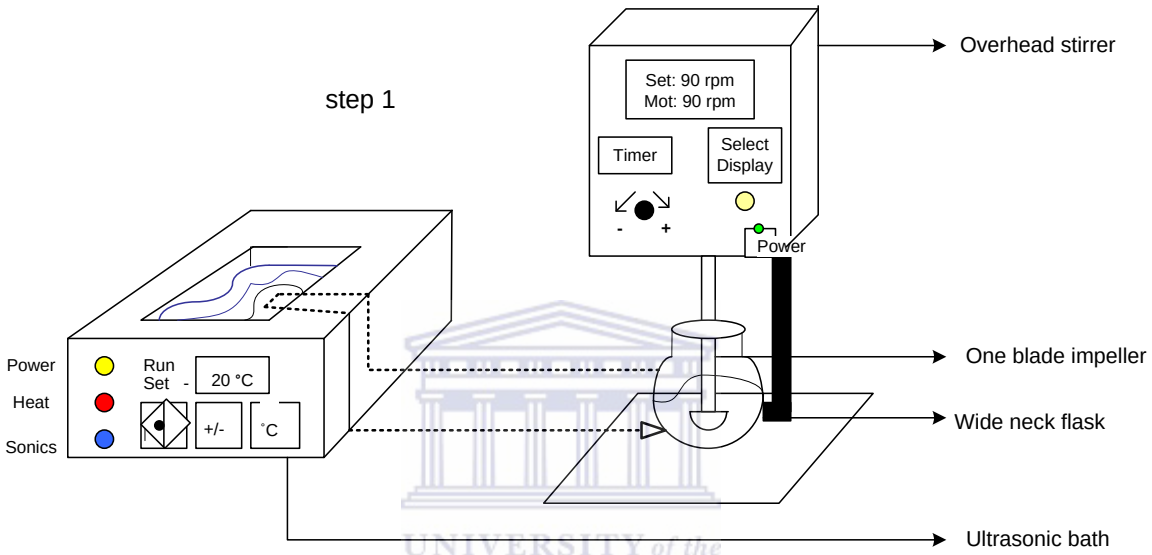

Figure 3. 1 Schematic representation of spinning suspension

Table 3. 1 Suspension properties and spinning parameters for fibre 1-5

Fibre	Solvent composition (NMP/water) wt%	Spinning mixture (wt %)					Viscosity at 20/s (Pas)
		NMP	PES	Particles	PVP	Water	
1	100/0	38.5	6.0	55.0	0.5	0.0	28.5
2	94/4	37.8	5.9	54.1	0.5	1.6	32.3
3	92/8	37.3	5.8	53.2	0.5	3.2	35.7
4	88/12	36.6	5.7	52.3	0.5	5.0	39.9
5	100/0	50.4	16.9	31.7	1.0	0.0	43.0

3.2.2 Extrusion

The degassed mixture containing YSZ powder was transferred into a dispensing vessel and pressurized at different gauge pressure of 1-2.5 bar using nitrogen gas (Fig 3.3, step 2A). The spinning suspensions were extruded through a triple-orifice spinneret into the coagulation bath. The schematic diagram of the spinneret used in this study is shown in Fig 3.2 where the dimensions of the inner and outer orifices and the inner tube are given in the insert. The internal coagulant was supplied to the injection capillary of the spinneret through a pump at a flow rate of between 0.05-0.3ml/s. De-ionised water and a mixture of de-ionised water/NMP was used as the internal coagulant. Figure 3.3 depicts a simplified diagram for preparation of hollow fibre membrane using phase inversion method.

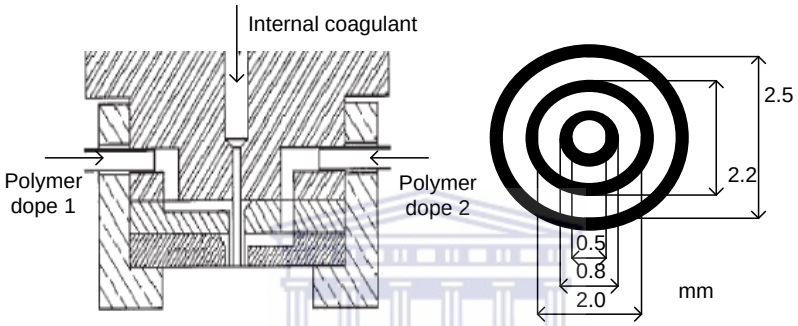

Figure 3. 2 Triple-orifice spinneret [106]

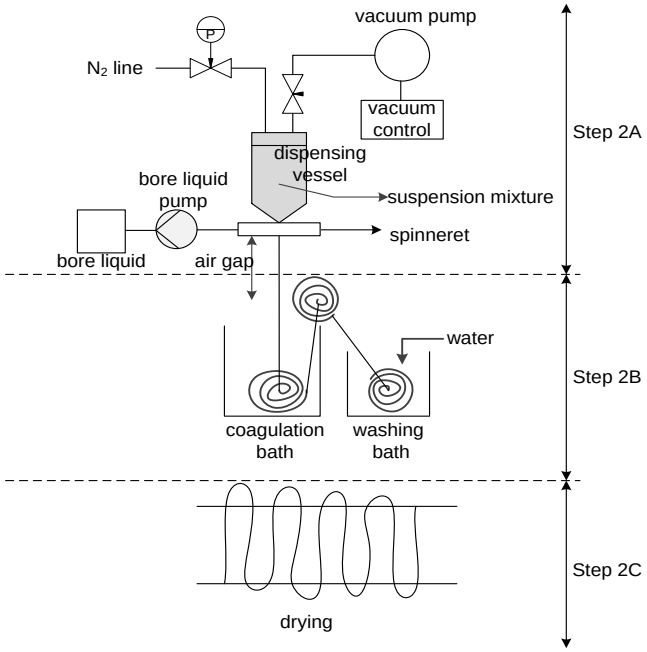

Figure 3. 3 A simplified diagram for preparation of hollow fibre membrane using phase inversion method [114]

3.2.3 Coagulation

After extrusion, the pre-nascent fibre passed through an air gap of between 3cm and 25cm before being plunged into the coagulation bath. The coagulation bath used in this study was 50cm long. The formed precursors were passed through a water bath to complete solidification for 24 hours, shown in Fig 3.3 (step 2B), followed by drying and stretching for 24 hours to straighten the fibre (Fig 3.3, step 2C).

3.2.4 Sintering

Dried precursors (25cm long) were placed into the ceramic quartz and calcined in air to yield ceramic hollow fibre membranes. The temperature was increased from 25 °C to 600 °C at a rate of 2 °C/min and maintained at its temperature for 3 hours to remove the polymer matrix by thermal and oxidation decomposition. The temperature was further increased to 1250-1450 °C at 5 °C/min and maintained at its temperature for 10 hours for final sintering. The temperature was reduced to 25 °C at a rate of 5 °C/min. A picture of a tubular furnace and firing schedule is shown in Fig 3.4a-b, respectively.

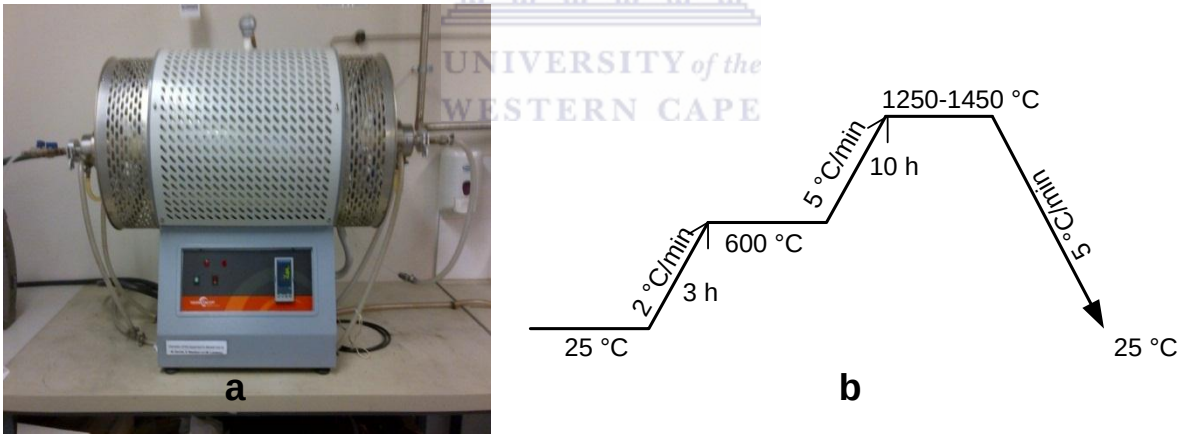

Figure 3. 4 (a) Schematic representation of a tubular furnace and (b) Firing schedule

3.3 Membrane characterization

Proper characterization of the support structure is very crucial. This usually involves measurements of particle size (Zetaziser), rheological properties (Viscometer), morphology and permeation. Ceramic hollow fibre membranes were characterized so as to give insight into the expected outcomes of the experimental investigations. Analysis of membrane provides information necessary to monitor membrane production and it is important for both membrane users as well as manufactures.

Generally, the characterization techniques for ceramic hollow fibre membranes are classified according to their morphology and permeation. The morphology or related parameters can be characterised by different techniques such as scanning electron microscopy (SEM) or field emission scanning electron microscopy (FESEM), transmission electron microscopy (TEM), atomic force microscopy (AFM). The permeation related parameters can be characterized by mercury porosimetry, bubble point technique, permporometry. In this study, hollow fibre membranes were characterized by techniques presented in the following subsection.

3.3.1 Zetaziser

Zetaziser is a valuable instrument in the research and development of materials. Zetaziser is capable of the identification of single and multi-phases in unknown materials quantification thereof, determination of the crystallographic structure of material, structure refinement and deformation.

For the purpose of this study, Zetaziser (Malvin Instrument) which uses photon correlation spectroscopy with a measuring diameter in the range of 5-5000nm was used to measure the particle size. In order to determine the minimum time needed to fabricate YSZ dope, a spinning suspension was prepared by adding the YSZ particles into NMP, followed by stirring for 15min. A certain amount of NMP was poured into a cuvette up to 1cm. A droplet of the stirred mixture was added into cuvette for zetaziser measurement. To decrease the amount of agglomerates, ultrasonic treatment was applied for preparation of YSZ. Zetaziser measurements were taken every 15 minutes of sonication.

3.3.2 Viscometer

To determine the rheology of non-Newtonian and time-dependent behaviour, rotational viscometer is essential. The technique is used to shear the sample between the two parts of measuring device by means of rotation. In agitation, the rotational speed is proportional to the shear rate [115].

In this study, the basic rheological measurements were carried out with a single-spindle viscometer (Brookfield Viscometer DV-11+Pro). A spindle attached to an instrument with a vertical shaft was rotated in the 50ml beaker containing spinning suspension (fibre 1-5, Table 3.2) and the force necessary to overcome the viscous resistance was applied (apparent viscosity against rotational speed). The spindle (RV6 type) was rotated at different speed (0.3-150RPM).

3.3.3 Scanning electron microscopy (SEM)

In scanning electron microscopy (SEM), electron probes are used to form an image instead of light. The interaction between the primary beams and specimen produces various signals from back scattered electrons. In order to obtain the signal induced by electron bombardment, the sample needs to be conductive. Non-metallic samples such as ceramics have to be coated, i.e platinum or gold. This type of technique can only give qualitative information about the membrane morphology. A drawback of this technique is that the resolution is not good enough at magnifications higher than 10^5 times [1]. The advantages of SEM is that it has less stringent sample preparation requirements resulting in examination of a largely unaltered state since the required property for SEM is a conducting surface layer.

In this study, the structures of prepared hollow fibre membranes were investigated using a scanning electron microscope, AURIGA HR (ZEISS). To observe cross section of the hollow fibre membrane by SEM, the dried green membrane was first immersed in liquid nitrogen for approximately 5min; the frozen membrane was slowly flexed until a clear cross section fracture occurred. The cross section of the sintered hollow fibre membranes was obtained by sharp snapping. These membrane samples were placed on the metal holder and were gold coated using a sputters coating operated under vacuum. The SEM images were taken at various magnifications.

3.3.4 Atomic force microscopy (AFM)

Atomic force microscopy (AFM) is a versatile imaging technique capable of producing three dimensional surface images. This type of technique uses high resolution scanning probe. It consists of a silicon cantilever with the sharp tip radius at the end [116]. AFM can produce images of materials as small as 1nm. The advantage is that no membrane retreatment is required but disadvantages area that rough surface may be difficult to interpret [117].

In this study, the surface roughness of the hollow fibre membranes was determined by AFM (nanoman). Three dimensional surface images were obtained in tapping mode using a silicon probe (MESP-sensor). The MESP probe had a resonance frequency of 60-100 kHz with a cantilever length of 200-250μm. Small pieces of ≤1cm ceramic fibres were attached to a magnetic disc with white double sided tape to allow for imaging of surfaces.

3.3.5 Mercury porosimetry

Mercury porosimetry is one of the fastest methods for determining pore size and pore size distribution in membranes. In mercury intrusion porosimetry, non-wetting mercury is used to gain information on the porous structure of a membrane. Usually, mercury is forced into a dry membrane at different pressure with the volume of mercury intruded determined at each pressure. Blind and closed pores are included into the pore size and pore size distribution of the membrane structure, however the permeability of the membrane is determined by only open pores [1, 118].

The pore diameter and pore size distribution were measured by mercury porosimeter (Autopore IV 9500). Small pieces of ≤1cm ceramic fibres were placed in a penetrometer followed by loading it into the instrument. This was operated at both low and high pressure intrusion.

3.3.6 Permeation measurements

In industrial plants, membrane modules are arranged in different ways based on the membrane processes. Dead-end module is one of the simplest operation in industry today. In dead-end, the flows of the feed stream and the permeate are both perpendicular to the membrane surface [15].

In this study, single gas permeation experiments were carried out with pressure control using gas. One end of the ceramic hollow fibre membrane was sealed and placed in a stainless steel tube for collecting the permeating gas. The remaining open end was connected to the feed gas. The gap between the hollow fibre membrane and the stainless steel was sealed with Pattex glue to avoid leakage of gas. A soap bubble flow meter was used to measure the permeating flow, shown in Fig 3.6. Prior to the permeation test, the membrane seal was tested in water as shown in Fig 3.7, followed by heat treatment at the temperature of 80 °C for 4 hours.

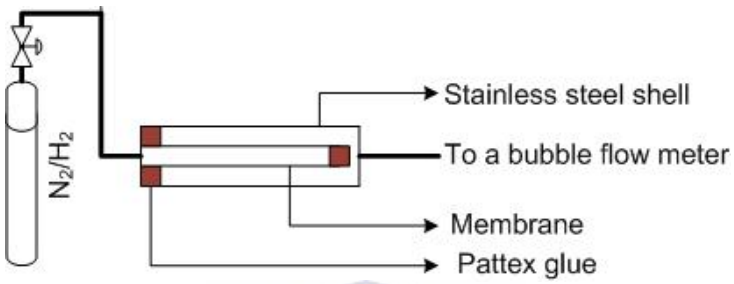

Figure 3. 5 Diagram of apparatus for gas permeation [16]

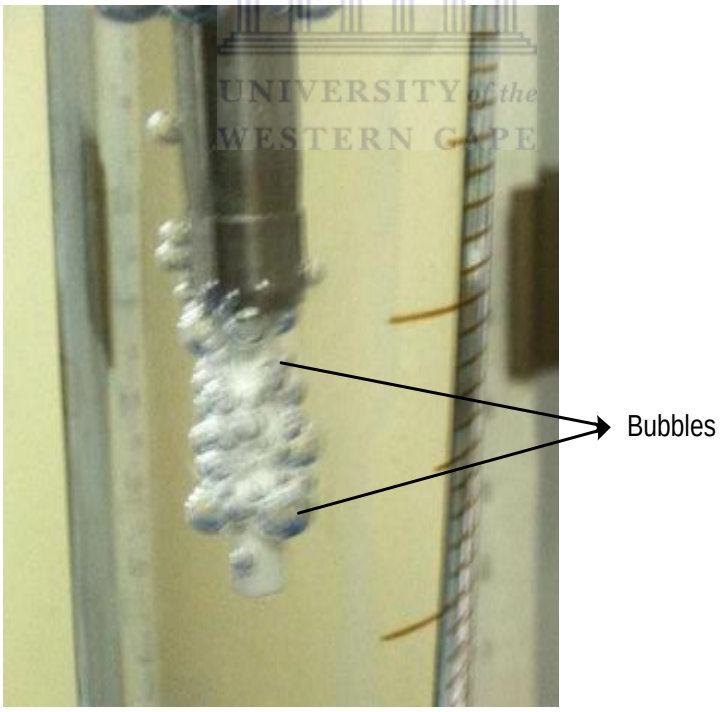

Figure 3. 6 Membrane seal test

Chapter 4

4. Results and Discussion

The results obtained from the experiments (Chapter 3) are discussed based on the particle size, spinning parameters, morphological transformation of ceramic hollow fibre membranes during various stages of synthesis; rheology, particle loading, sintering temperature and altering the concentration of the internal coagulant. YSZ hollow fibre supports which have both symmetric and asymmetric structure were prepared by the phase inversion method. Both structures were obtained according to literature. The initial step undertaken in developing a successful high performance support for palladium based membrane was to formulate a spinning suspension and analyse the particle size of YSZ.

The particle sizes of the YSZ solution were analysed to ensure uniform dispersion. The curve below (Fig 4.1) shows the duration necessary to fabricate reasonable YSZ solution dispersion for Zetasizer measurement. The ultrasound bath achieved the highest zetasizer peak at time 0 min, shown in Fig 4.1a. This is likely due to the soft agglomerates of YSZ powder that were added into the spinning suspension and hence trap air in the interstitial space between the primary particles. This is considered unfavourable as the trapped air would produce bubbles in the membrane precursor, hence resulting in pin holes and unwanted surface porosity in the final sintered support. A decrease in particle size with increasing ultrasonic time to 15 minutes is observed.

The trend of decreasing zetasizer peak may be attributed to increasing the ultrasonic time which caused the YSZ soft agglomerates to dislodge from the matrix. Zetasizer peaks from 30-60min showed an even distribution of particles throughout the solvent. This implies that the particles will continue to stabilise to infinity, which was not achieved in the test time. It is deduced then that up to this point the ultrasonic bath very effectively homogenises the YSZ particles and prohibit soft agglomerates from reforming in the spinning suspension. From the observation of YSZ suspension that has been prepared to analyse the particle size, it is clear that the particle size of the suspension decrease with increasing sonication time. This observation is reported by Luiten-Olieman *et al.* [70]. Two tests were taken to confirm the validity of using the ultrasonic bath in protecting and stabilizing what has been accomplished. Fig 4.1b thus behaves as expected. The tests were carried out at the set temperature of approximately 20 °C.

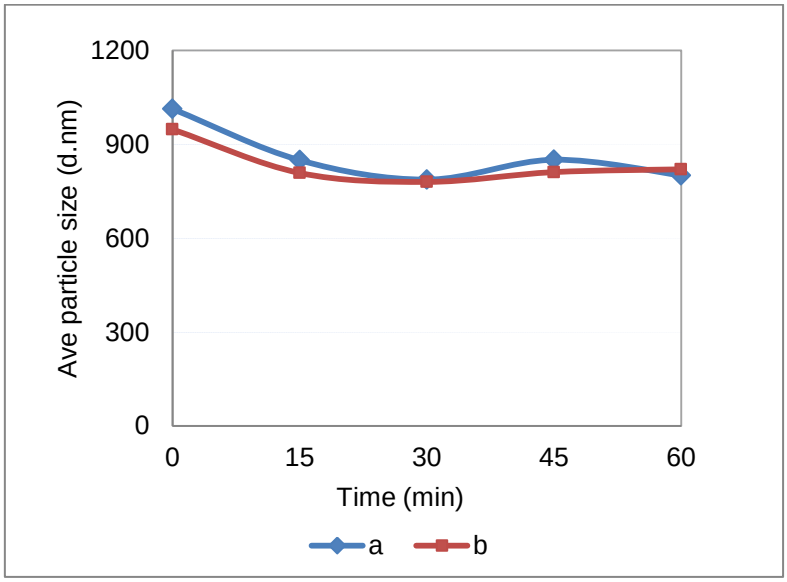

Figure 4. 1 Particle size distribution of YSZ

The second step of the experiment was to examine spinning parameters with the idea of developing certain parameters which could predict the fibre dimension from a set of spinning parameters. Spinning parameters are variables that establish the geometry of the hollow fibre membranes, such variables include: bore liquid flow rate, pressure and air gap [119]. The data used to test the validity of these sets of variables were obtained from spinning parameters in which all variables were kept constant except for the one under examination. The spinning of hollow fibre process is, in reality, much more complicated, due to slow kinetic and thermodynamic features related to the viscosity of the polymer solution [13, 116]. The examination of spinning parameters shows some of the problems encountered by spinners during synthesis. In this study, the effect of spinning parameters on the hollow fibre precursor was studied in a qualitative manner using the spinning suspension containing NMP 50.4 wt%, PESF 16.9 wt%, PVP 1 wt% and YSZ 31.7 wt%. Spinning parameters which were examined are discussed in the following section.

(a) Bore liquid flow rate

It has been reported that the rate at which an internal coagulant is injected through the spinneret determines the size of finger-like voids near the inner wall of the hollow fibre membrane [120]. Increasing water injection rate has a huge effect on the hollow fibre membrane structure, except where the internal pressure is insufficient to cause rupture of the hollow fibre membrane wall when a low polymer extrusion is used. During the experiment the air gap (3cm) and pressure (2bar) were both kept constant except for the bore liquid flow rate. A visual comparison of the SEM results is depicted in Fig 4.2a-b. The

images shows that increasing the bore flow rate from 0.11ml/s (Fig 4.2a) to 0.3ml/s (Fig 4.2b), widen the intensity of the finger-like voids near the inner wall (region marked with the black shape). An increase in bore liquid flow rate extended phase separation time prior to solidification, and promoted the polymer lean phase growth and big finger-like voids (Fig 4.2b). These findings were similar to those observed by Wang *et al*. [120]. Benjamin and Kingsbury [56] studied the effect of bore liquid flow rate on the membrane morphology of Al_2O_3 hollow fibres. They noted that finger-like voids decreased in fibres prepared with increased flow rate. In this study, an increase in the internal coagulant flow rate promoted viscous fingering.

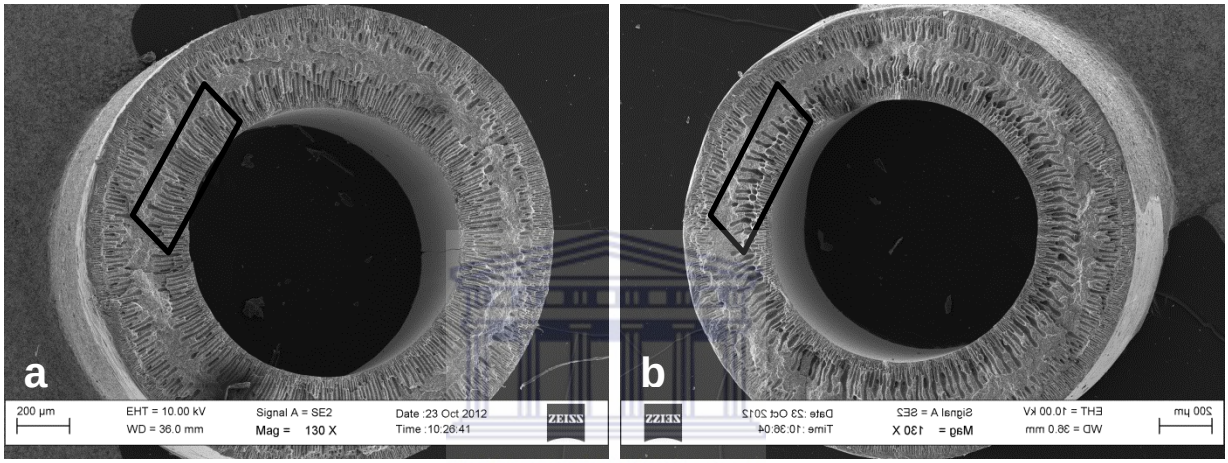

Figure 4. 2 Internal coagulant flow rate: (a) 0.11ml/s and (b) 0.3ml/s

(b) Air gap

In the hollow fibre membrane synthesis, the air gap can be described as the distance between the spinneret and the coagulation bath. The air gap condition has a significant influence on the morphology of the hollow fibre membrane because it is a point where the precursor formation starts. This topic has been investigated by many researchers and the effect on its morphology and permeation properties reported with conflicting observations. Although the effect of air gap has been investigated, a further study needs to be performed in order to verify if the conclusion applies for YSZ spinning suspensions.

Given that the air gap was the only variable that was under examination, the bore liquid flow rate (0.11ml/s) and pressure (2bar) were kept constant. Initially, the air gap was set to 3cm and later increased to 15cm. The diameter of the finger-like voids of the hollow fibre membrane spun with an air gap of 3cm (Fig 4.3a) were found to be similar to those of the other hollow fibre membrane prepared with the higher air gap of 15cm (Fig 4.3b). However it is evident that the ID and OD of the hollow fibre membranes are influenced by the increase

in air gap. The SEM image depicted in Fig 4.3b shows that both the ID and OD are slightly reduced by increasing the air gap length. Table 4.1 list the summary of the average outer and inner diameters of the precursors.

Table 4. 1 Effect of air gap on the inner, outer diameter and wall thickness of precursors

Fibre 5	Air gap (Bar)	Diameter (μm)		Wall thickness (μm)
		Internal	External	
Fig 4.3a	3	1154.5	1842	687.5
Fig 4.3b	15	1094.5	1760	665.5

Wei *et al*. [63] prepared YSZ hollow fibre membranes using an air gap length beyond 15cm. Their results showed a decrease in finger-like voids at the outer surface of the hollow fibre membranes and no variation in the inner fibre diameter. They stated that an air gap longer than 15cm absorbed moisture from air inducing phase inversion of the polymer binder. Therefore, the viscous fingering may not be possible to establish, as solidification of the outer surface takes place before immersing the nascent fibre into the external coagulant bath.

It must be mentioned that during the formation of hollow fibre membrane, gravity influences the minimum stretch ratio (e.g. ratio of take-up speed to dope extrusion speed) achievable in the spin line and hence introduces prolongation stress on the fibre. Chung and Hu [121] noted a decrease in diameter both in the inner and outer surface of polyethersulfone hollow fibre membranes with an increase in the air gap length. They too stated that the air gap introduces a longitudinal stress on the hollow fibre membranes because of gravity.

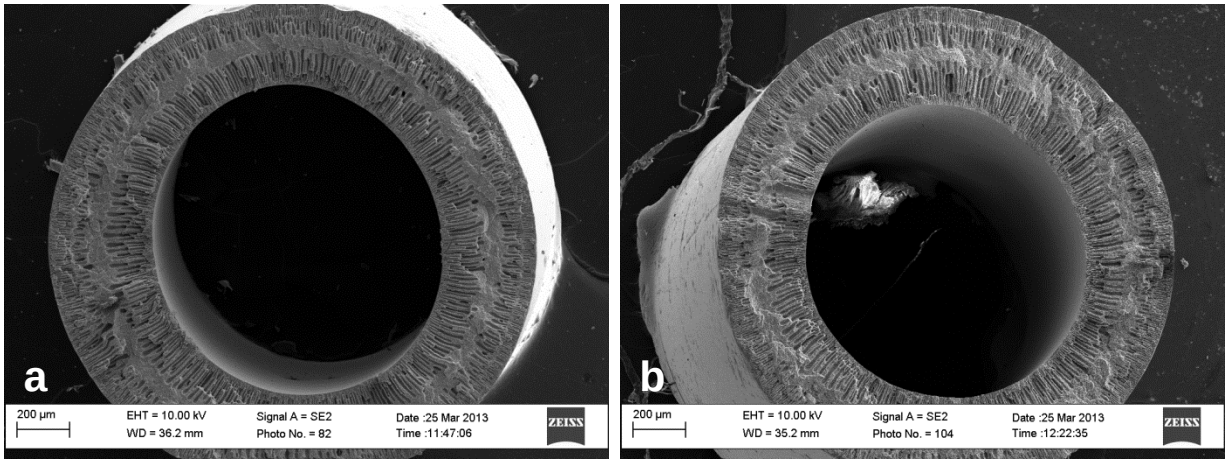

Figure 4. 3 Air gap: (a) 3cm and (b) 15cm

(c) Pressure

Dope extrusion rate is one of the primary variables that highly affect the inner and outer diameter of hollow fibres membranes as well as the thickness of the fibres. During the experiment the bore liquid flow rate (0.11ml/s) and the air gap (3cm) were both kept constant, while the pressure was varied. The YSZ precursors were extruded at different pressures and the resulting dimensions are summarized in Table 4.2.

Table 4.2 Effect of pressure on the inner, outer diameter and wall thickness of the precursors

Fibre 5	Pressure (Bar)	Diameter (μm)		Wall thickness (μm)
		Internal	External	
Fig 3.4a	1	831.9	1539.5	702
Fig 3.4b	2.7	1192	1927	735

The inner and outer diameter of the hollow fibre membranes as well as the wall thickness extruded at the pressure of 1bar shown in Fig 4.4a were smaller than those of the other hollow fibre membranes extruded at the pressure of 2.7bar (Fig 4.4b). Ismail *et al.* [122] studied the effect of dope extrusion rate on performance of hollow fibre membranes and gas separation performance. Their results suggest that as dope extrusion rate increases, the selectivity increases until a critical level of shear is reached beyond which the membrane performance deteriorates. Shilton *et al.* [123, 124] reported that both gas permeability and selectivity were enhanced with increasing dope extrusion rates.

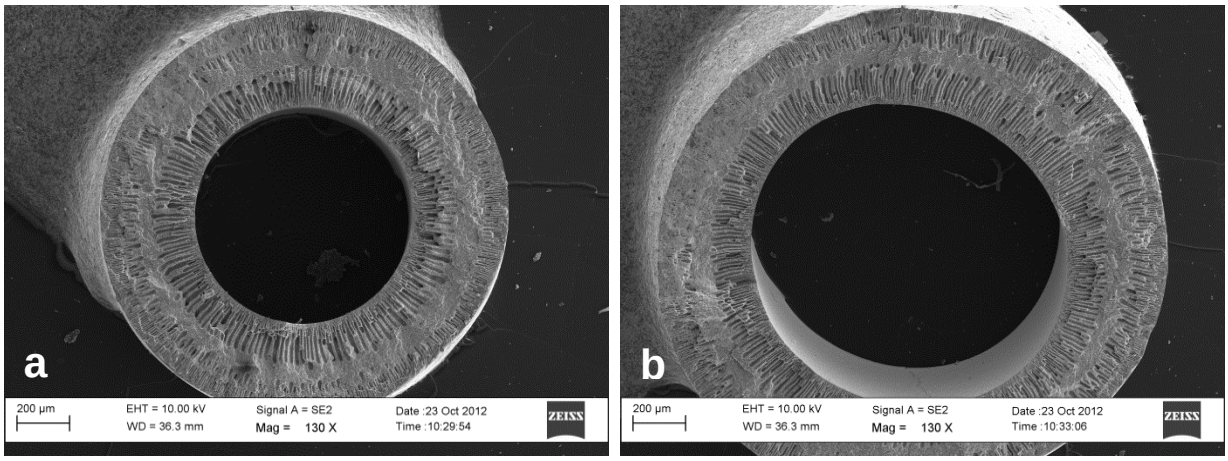

Figure 4. 4 Pressure: (a) 1bar and (b) 2.7bar

After several preliminary experiments, the following spinning parameters were adopted because they produced desirable properties: air gap (3cm), bore liquid flow rate (0.11ml/s) and pressure (1bar). All following experimental results were conducted based on the aforementioned spinning parameters. The morphology of YSZ support was not influenced by spinning parameters only but loading of particles as well. In order to gain insight into the effects of the fibre geometry on the hollow fibre membrane strength, loading of YSZ particles into the spinning suspension was investigated.

Fig 4.5 depicts SEM images spun from spinning suspension containing YSZ 29 vol% (Fig 4.5a-e) and 66 vol% (Fig 4.5f). The presence of defects is due to low particle loading (29 vol%) during the preparation of the spinning suspension, thus making it difficult to obtain smooth precursors (as shown in Fig 4.5a). Figure 4.5b-e illustrates the microstructure of sintered hollow fibre membranes. The sintering process was carried out at the temperature of 1450 °C for 1 hour. It can be seen from the micrograph of Fig 4.5b that during sintering treatment, the fibre breaks up into short pieces that result in a partial fibre (Fig. 4.5e). Breakages of fibre in Fig 4.5b led to separation of two layers, indicating bad adhesion (Fig 4.5e).

Morphology of the asymmetric YSZ layered surface is shown in Fig 4.5c-d. A thin skin layer is integrated on the porous support of the same ceramic material (Fig 4.5c) and Fig 4.5d further confirms that such a layered ceramic membrane can be prepared in one step. At 29 vol% YSZ concentration, numerous defects were found to be present. However, increasing the concentration of the YSZ resulted in a good, even hollow fibre membrane with better mechanical strength (Fig 4.5f). It was not possible to test the fibre that is shown in Fig 4.5e due to strength but the fibre that is depicted in Fig 4.5f was tested and hence used as a standard to investigate the effect of water in the spinning suspension, the findings are elaborated in detail in the following subsection. It is shown that the extent of deformation is directly related to the particle loading. The result agreed with the findings of Wei *et al*. [63] and Li *et al*. [91].

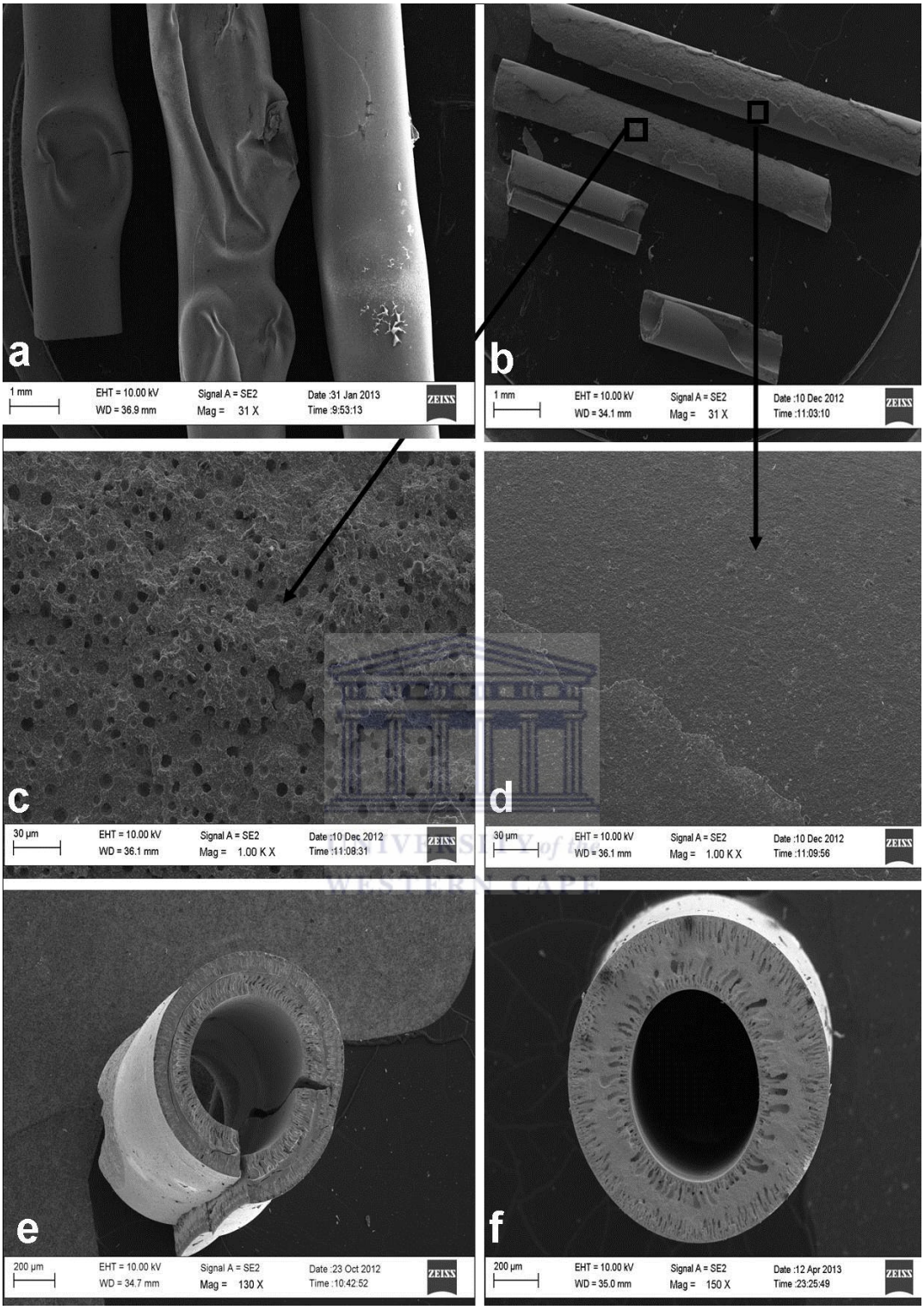

Figure 4. 5 Particle loading: Images of YSZ fibres with 29 vol%: (a) precursor, (b-e) sintered fibres and YSZ 66 vol% (f) sintered

A generally observed phenomenon is that the viscosity increases with the increase in particle contents or adding some additives in the spinning suspension. To examine the results of viscosity on fibre morphology, water and PVP were both used as additives to enhance the suspension viscosity. The material properties of the prepared membranes were measured by varying the solvent systems and polymer dope concentration that is closer to phase separation. Analysis indicated that addition of such additives highly affect the properties of the membrane. The addition of water to spinning suspension caused an increase in viscosity as depicted in Fig 4.6a.

The viscosity of spinning suspension containing 0wt% water was 28.5Pa.s, further addition of water to 4wt%, 8wt% and 12wt% resulted in a viscosity of 32.3Pa.s, 35.7Pa.s and 39.7Pa.s, respectively. Fig 4.6b illustrates the viscosity of YSZ loaded spinning suspension against shear rate. The graph display a pseudo-plastic fluid whose apparent viscosity increase with a decrease in shear rate. The observation correlates with the findings of Luiten-Olieman *et al*. [106], Benjamin and Kingsbury [56] who both reported that the suspension viscosity increases more rapidly when it is in contact with the non-solvent or when the polymer phase is closer to its precipitation point.

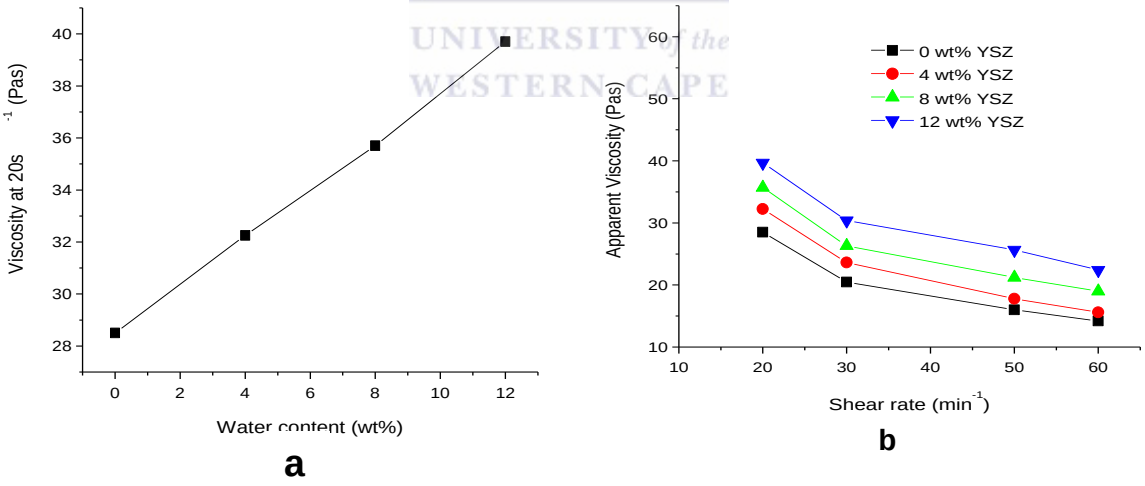

Figure 4. 6 Viscosity of spinning suspension prepared with 0-12wt% water

The cross-sectional structures displaying the effect of water content on the membrane morphology of YSZ hollow fibre supports are shown in Fig 4.7. SEM micrographs depicted in Fig 4.7 were prepared from different starting suspension containing 0wt%, 4wt%, 8wt% and 12wt% water content. Fig 4.7a shows a cross section of the asymmetric structure of the YSZ prepared with 0wt% water content. The formation of long finger-like structures in the inner

and outer surface of the fibre may be due to the rapid precipitation which occurs during the spinning process.

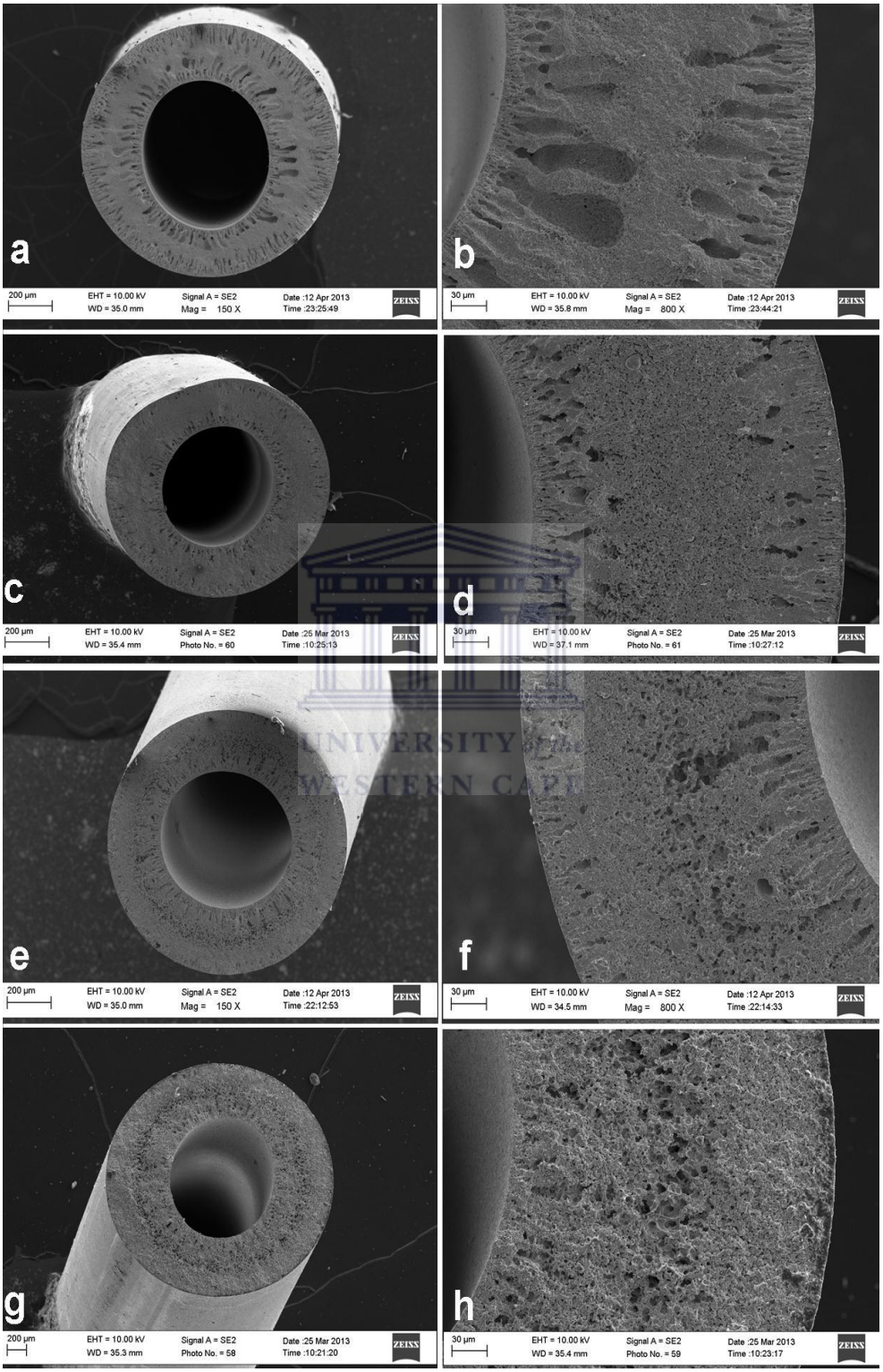

Figure 4. 7 SEM pictures of YSZ hollow fibre membranes prepared from dope containing varying amount of water (a): fibre 1, 0wt% water, (b): enlargement of fibre 1, (c): fibre 2, 4wt% water, (d): enlargement of fibre 2, (e): fibre 3, 8wt% water, (f): enlargement of fibre 3, (g): fibre 4, 12wt% water (h): enlargement of fibre 4

An image (Fig 4.7b) with higher magnification of the cross section confirms that these finger-like structures extend almost to the centre of the fibre cross section, where a spongy-like structure exists. This is considered unfavourable, as finger-like structure negatively influence the mechanical strength of the fibre. Finger-like structures reduce the mechanical strength of ceramic hollow fibre membranes, hence elimination of finger-like structures is important [16]. Fig 4.7c shows a slight reduction in finger-like structure length with increasing water content to 4wt% in the YSZ spinning suspension. Finger-like structures are developed more in the inner surface with comparison to the outer surface of the fibre, Fig 4.7d. This structure is attributed to several factors, such as the viscous fingering phenomenon, movement of particles and the forming precursor is exposed to the internal coagulant bath first before the external coagulant bath. When the water in the internal coagulant is in contact with a highly viscous YSZ suspension, the hydrodynamic unstable viscous fingering takes place [16, 90].

Fig 4.7e illustrates a small reduction in finger-like structure length at 8wt% water content and at higher magnification, shown in Fig 4.7f. This type of fibre showed similar results in comparison to the fibre depicted in Fig 4.7c-d. This difference in morphology is likely related to the increase in the amount of water required to stimulate phase transition of spinning suspension or the rate of viscous fingering which is slightly closer to the rate of phase inversion. According to Wang *et al.* [98], Strathmann [125], Young and Chen [103], spinning mixtures with composition closer to the phase inversion results in the formation of sponge-like structures. This would explain the results obtained in Fig 4.7g-h where a definite sponge-like structure exists at the centre and extends fully to the outer and inner edge of the fibre with the addition of 12wt% water content. This type of fibre has the potential to withstand high pressure. An increase in suspension viscosity inhibits viscous fingering at both the inner and outer surface of the fibre as was observed by Benjamin and Kingsbury [56]. It was decided not to continue spinning the dope containing 16wt% water content due to breakage during spinning.

The outer surface area of the ceramic support was investigated using AFM and SEM images. AFM images of the resultant hollow fibre membranes as shown in the left hand side (Fig 4.8) and SEM images shown in the right hand side, illustrate the difference in morphology between different batches of different water content: 0wt%, 4wt%, 8wt% and 12wt%. In order to obtain the roughness of the hollow fibre support from AFM images, Nanoscope, V720 was used to calculate the roughness of the membrane in terms of mean roughness (Ra) and root mean square roughness (Rq) as shown in Table 4.3. Fig 4.8a, c, e & g shows the three dimensional AFM images of the YSZ membrane outer surface obtained in 5µm x 5µm scaling area using a 900nm Z range.

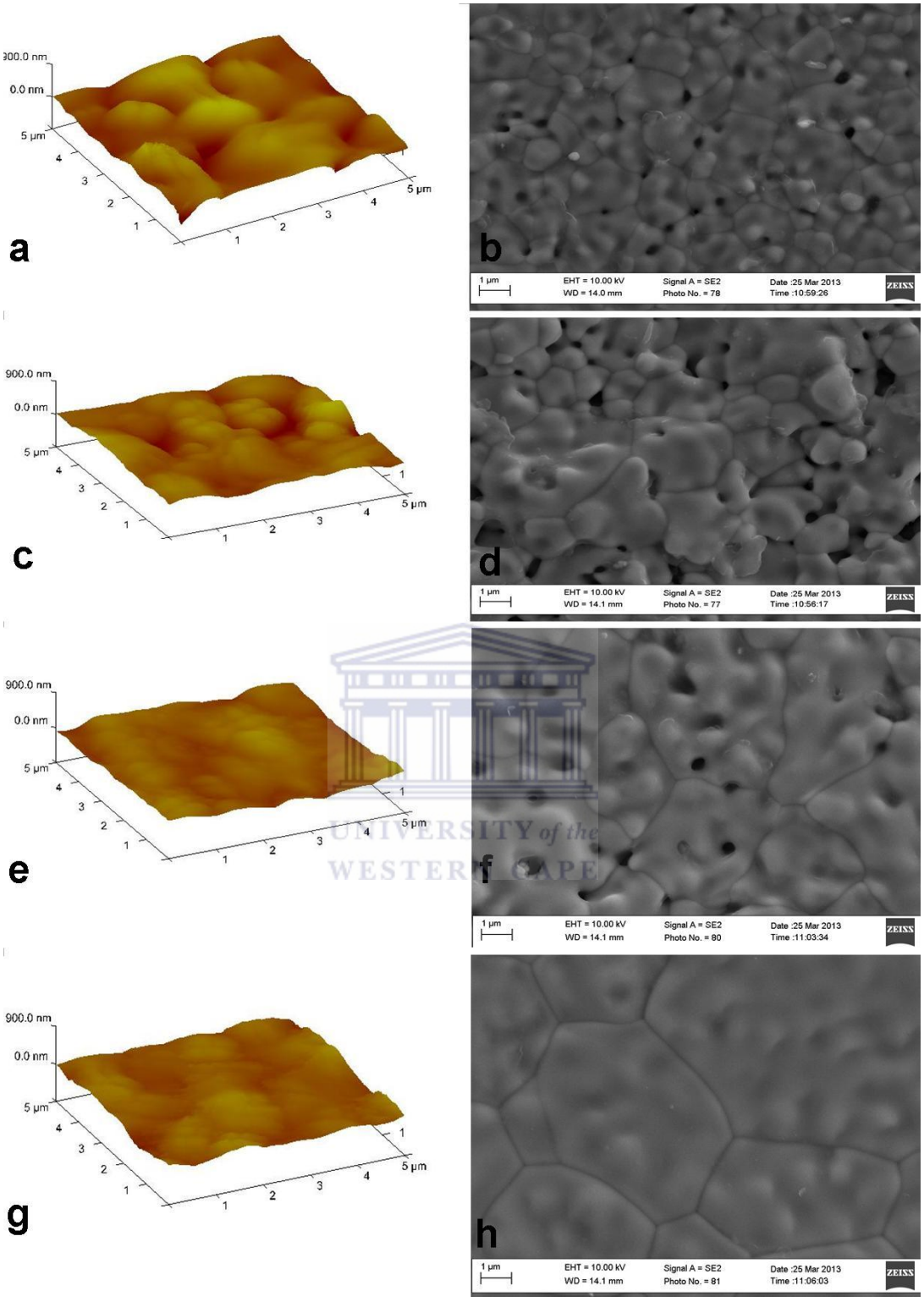

Figure 4. 8 3D AFM images (a, c, e & g); SEM images (b, d, f & h) of outer surface prepared from dope containing varying amount of water (a-b): fibre 1, 0wt% water, (c-d): fibre 2, 4wt% water, (e-f): fibre 3, 8wt% water, (g-h): fibre 4, 12wt% water

Table 4. 3 Roughness parameters of YSZ hollow fibre membrane

Fibre	Mean Roughness Ra (nm)	Root Mean Square Roughness Rq (nm)
a	89.9	111
c	68.7	91.2
e	47.1	58.5
g	45.5	56.4

It can be noted that the roughness parameters for the membrane prepared with 0wt% water content in the spinning mixture is high (Fig 4.8a, Table 4.3), and several open pores can be observed (Fig 4.8b). As the water content is increased to 4wt%, 8wt% and 12wt% in the spinning mixture, the roughness parameters decrease (Fig 4.8c, e & g, Table 4.3) and the outer surface becomes even denser. The SEM images show an increase in grain growth and decrease in porosity as given in Fig 4.8d, f & h. Singh *et al.* [126], Bessieres *et al.* [127] and Fritzsche *et al.* [128] reported that the change in the roughness parameters is proportional to the change in pore size.

When AFM images contain high peaks that correspond to the nodules, high roughness parameters are expected. The highest roughness parameters were obtained for the membrane illustrated in Fig 4.8a. The porosity of this membrane is much higher than the porosity of the membrane illustrated in Fig 4.8c, e & g. Fig 4.8e and g clearly shows that the surfaces of the membranes are much smoother. This may be due to the influence in porosity, which is less in comparison to the membrane in Fig 4.8a and c. Membrane support with lower roughness has stronger antifouling abilities [97, 129]. Therefore, in order to improve antifouling ability, fabrication of membrane support with less roughness should be taken into account. It has been clearly shown in this study that the water content does have an influence on the porosity of the support structure.

To further verify the decrease in porosity with increasing water content in the spinning mixture, mercury porosimetry was used to measure the pore size distribution of the hollow fibre support. The results obtained indicate a multimodal distribution with a decrease in pore volume, shown in Fig 4.9. The hollow fibre membranes with 0wt% water content represent at least 42% of the total pore volume. Fibres with 4wt% water content led to a small reduction in the fractional volume, about 33% occupied by these pores. Further increase of water content to 8wt% led to a further reduction of approximately 20%, and addition of water to 12wt% resulted to an approximation of 5% reduction. This observation is in agreement with a literature report given by Luiten-Olieman *et al*. [106].

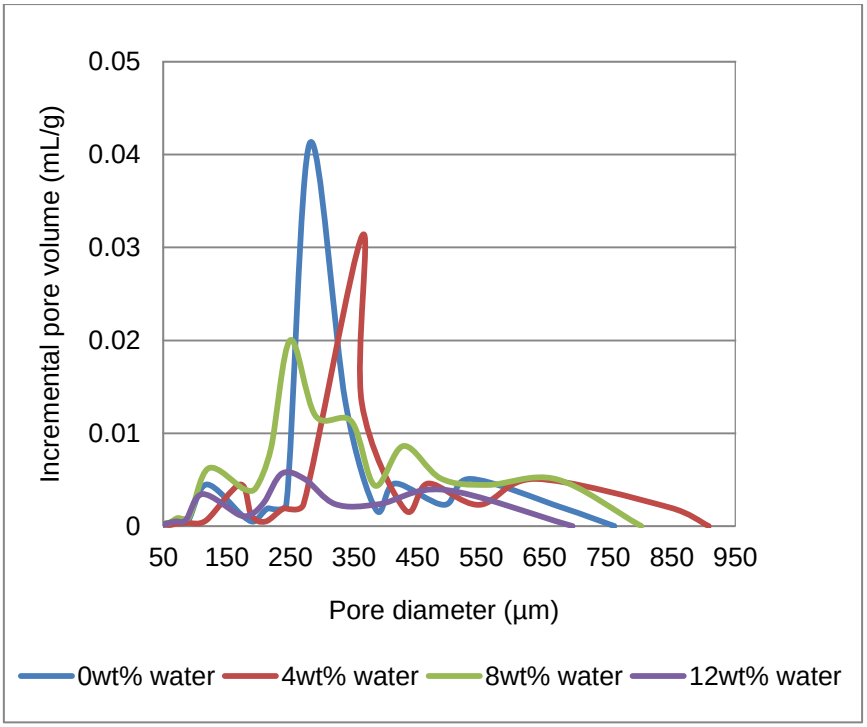

Figure 4. 9 Mercury intrusion data sintered at 1450 °C for 10h

The disadvantage of using this technique for pore analysis is that small pore size requires high pressures which may damage the membrane pore structures. The procedure determines all pores present in the hollow fibre membrane including dead end pores [1]. The decrease in pore volume shows a decrease in porosity but the decrease in mean pore diameter shows the decrease in pore radius. Fig 4.10 depicts the progressive densification of the sponge-like structure of the hollow fibre membrane support. The figure shows a linear increase in compressed air permeance with increased pressure difference across the hollow fibre. The gas permeance decreased with increasing water concentration. Membrane support with less roughness had less flux. This indicates the stability in terms of pore structure and physical properties of porous YSZ synthesized in this study. The uniform sponge like structure on the cross section and outer surface of the hollow fibre membrane derived from the spinning suspension that contains 12 wt% water content is beneficial for use as a membrane support for palladium based membranes.

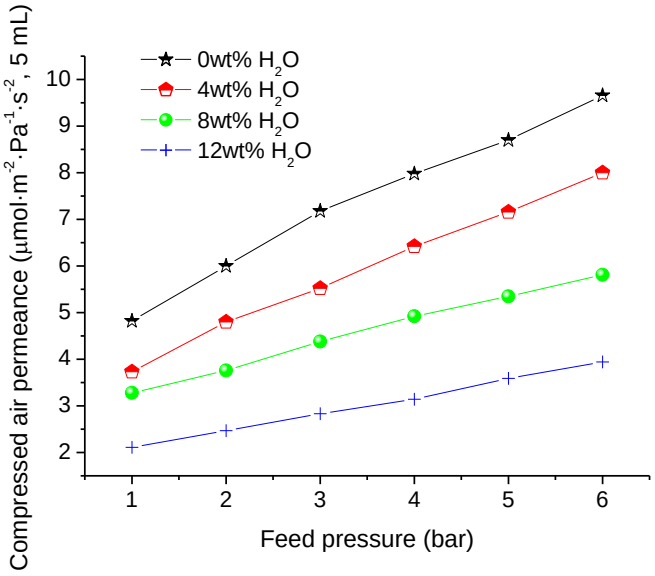

Figure 4. 10 Compressed air permeance as a function of feed pressure for support prepared from dope containing varying amount of water

The effect of sintering on the membrane morphology was further investigated. All fibre samples were prepared from the spinning suspension that contains NMP 38.5 wt%, PESF 6 wt%, PVP 0.5 wt% and YSZ 55 wt%. Fig 4.11 portrays development of the YSZ morphologies at different sintering temperatures between 1250 °C and 1450 °C for 10 hours. A more detailed analysis of the development of outer surface morphology with sintering temperature is shown in Fig 4.12. The cross section shown in Fig 4.11(A-a) seems very porous with the temperature of sintering as low as 1250 °C. A deeper analysis of the outer surface at a higher magnification reveals some significant difference. Fig 4.12a shows that irregular pores are evenly distributed on the surface.

Evident changes in the cross section take place at 1350 °C (Fig 4.11B-b), although the general structure is maintained, the surface of the fibre experience changes in shape and reduction in pore volume because of particle coalescence, the interconnected pores are still observed from the hollow fibre surface as shown in Fig 4.12b. When the temperature is further increased to 1450 °C, the cross section becomes almost dense (Fig 4.11C-c) with a significant increase in grain size (Fig 4.12c). From the observation that is shown in Fig 4.12, it is clear that the sintering temperatures play an important role for elimination and formation of pores. This observation correlates well with that of Wei *et al.* [63], who found that the porosity decrease with increasing sintering temperature up to 1500 °C.

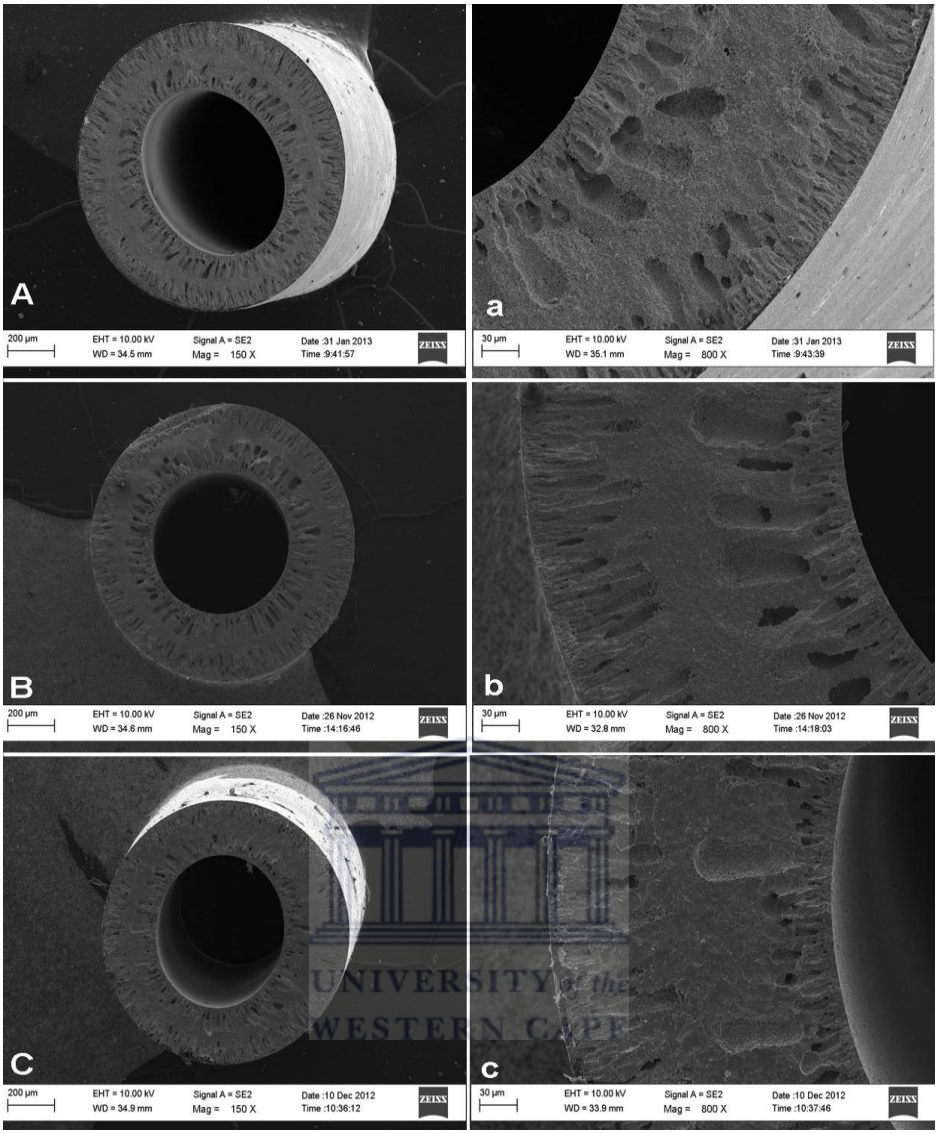

Figure 4. 11 SEM images of sintered fibres: (A-a) 1250 °C, (B-b) 1350 °C, (C-c) 1450 °C

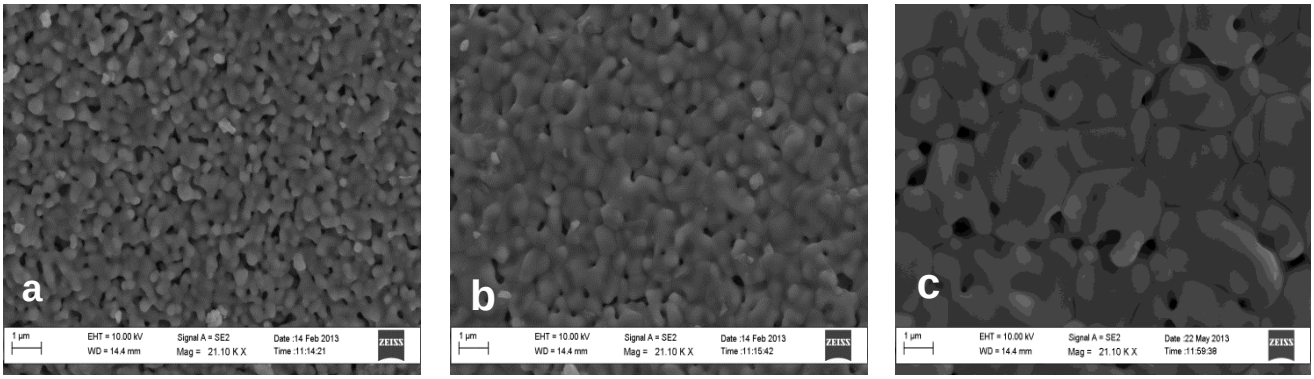

Figure 4.12 SEM images of the outer surface of the YSZ hollow fibre membranes sintered at 1250 °C (a), 1350 °C (b), 1450 °C (c)

A more detailed analysis of the development of the outer surface morphology with sintering temperature, determined with AFM is depicted in Fig 4.13. It can be seen that the surface of the membrane is not smooth and consist of high peaks (bright region) that correspond to the nodules/grain size and valley peaks (dark region) that correspond to the pore size.

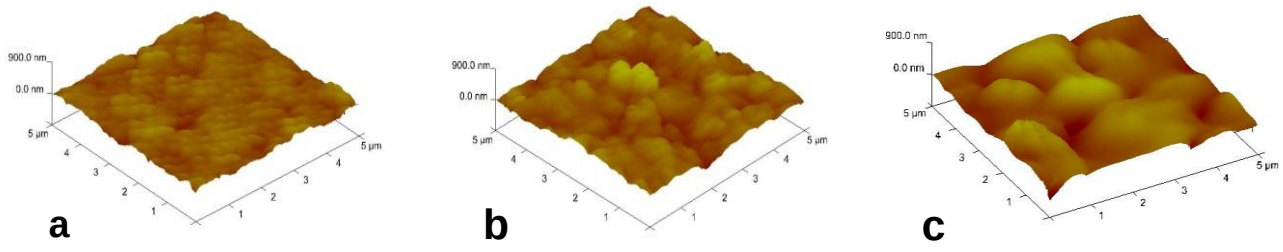

Figure 4.13 AFM images of the outer surface of YSZ hollow fibre membranes sintered at 1250 °C (a), 1350 °C (b), 1450 °C (c)

Fig 4.13a shows the 3D AFM image of the outer surface of a YSZ hollow fibre membrane sintered at 1250 °C, it appears that the grain size are in a row. On increasing the sintering temperature to 1350 °C and 1450 °C, the grain size of the outer surface of YSZ hollow fibre membranes increased. The roughness parameters are given in Table 4.4. From Table 4.4, it appears that the roughness parameters of the outer surface of the hollow fibre membranes decrease on higher heat treatment. Very similar results were reported by Wei *et al*. [63] and Jayaseelan *et al*. [130].

Table 4. 4 Roughness parameters of sintered YSZ hollow fibre membrane at different temperature

Sintered Fibres T (°C)	Mean Roughness Ra (nm)	Root Mean Square Roughness Rq (nm)
1250	89.9	111
1350	62.2	82.6
1450	45.3	56.9

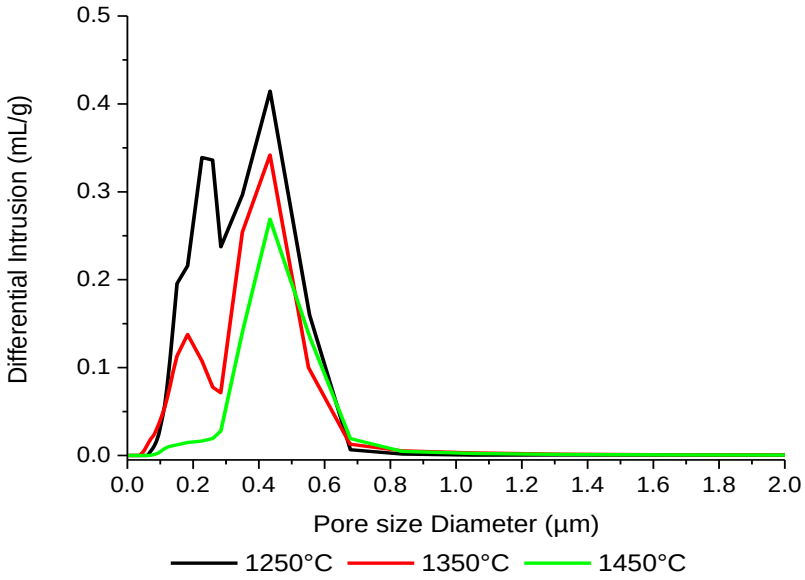

Figure 4.14 Pore size distribution vs. sintering temperature for asymmetric hollow fibre membranes

The reduction in porosity of the membrane support structure can also be observed in mercury intrusion data, shown in Figure 4.14. There was an overall decrease in pore volume with increasing sintering temperature. The fibre sintered at 1250-1350 °C shows a bimodal pore size distribution with a broader peak at approximately 0.5µm, which represents the pores near the inner wall of the fibre, and also form the entrance to the finger-like voids. A sponge-like structure is represented by a peak at approximately 0.35µm. Although a fibre sintered at 1350 °C shows bimodal pore size distribution, it can be seen that both finger-like structure and sponge-like structure are reduced. Sintering at a temperature of 1450 °C resulted in a reduction in porosity in both regions. The decrease in porosity with sintering temperature increase is due to pore shrinkage or densification of particles occurring at elevated temperature, especially when grain boundary and lattice diffusion occurs.

Despite the reduction in porosity and densification of sponge-like structure, it is clear that finger-like structures remain even at elevated temperature. This observation correlates with that of García-García *et al*. [131], Benjamin *et al*. [56] and Luiten-Olieman *et al.* [106]. The porosity of the sintered YSZ hollow fibre supports was further determined from the gas permeation test using compressed gas. Fig 4.15 shows the permeance for the support membrane prepared as a function of differential pressure. As noted below, a high permeation flux was obtained with supports sintered at lower temperature. The compressed air permeance shows a linear relationship with pressure difference across the supports in

temperature range 1250-1450 °C. As the sintering process is increased the gas permeation flux decreases. This observation is in agreement with data obtained by Benjamin *et al.* [56] and Pan *et al*. [71].

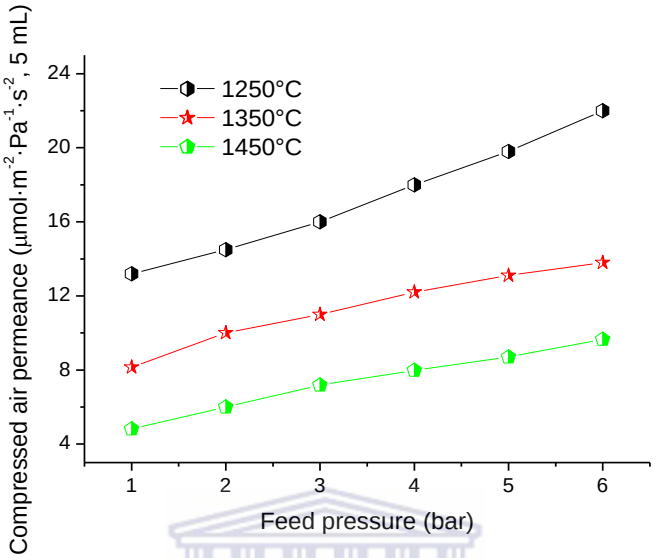

Figure 4.15 Compressed air permeance through YSZ support sintered at different temperatures

The last step of the experiment was to investigate the effect of the internal coagulation by coagulating the spinning suspension that contains NMP 38.5 wt%, PESF 6 wt%, PVP 0.5 wt% and YSZ 55 wt% in $100H_2O/100H_2O$ (internal/external), $60NMP:40H_2O/100H_2O$ and $90NMP:10H_2O/100H_2O$. This was done by changing the concentration of the internal coagulant while keeping 100wt% water at the external coagulant (Table 4.5). The membrane prepared using water in the external and internal coagulant showed finger-like voids in the inner and outer surface of the hollow fibre membrane (Fig 4.16a-b). Obvious changes in the cross sectional structure takes place when 60wt% NMP aqueous solution is used as the internal coagulant. The volume of the finger-like voids lengths near the inner wall of the fibre were reduced greatly (Fig 4.16c-d).

According to Kesting [132], finger-like voids structures are formed when the coagulant process is fast, however, slow coagulation result in a porous sponge-like structure. Additional increase of the NMP concentration up to 90wt% of the internal coagulant result in a sponge-like region near the inner wall (Fig 4.16e-f). This indicates that the solubility parameter difference between the nascent and the internal coagulant is small enough to prevent the occurrence of phase separation [16]. Wang *et al.* [133] used alcohol as an

internal coagulant. Their membrane exhibited greater permeation flux with the alcohol eliminating the inner skin layer of the hollow fibre membrane. It is evident that a fully sponge-like structure membrane can be produced if 90NMP:10H_2O/90NMP:10H_2O is used at the internal and external coagulant.

Table 4.5 Effect of internal coagulant

Fibre 1	**Coagulant (NMP: H_2O)**		**Morphology**		**Surface property**
	Internal	**External**	**Finger-like voids**	**Sponge-like pore**	**Defect amount**
A	0:100	0:100	Inner, outer	Middle	Minor
B	60:40	0:100	Outer, inner	Middle	A few
C	90:10	0:100	Outer	Middle, inner	Many

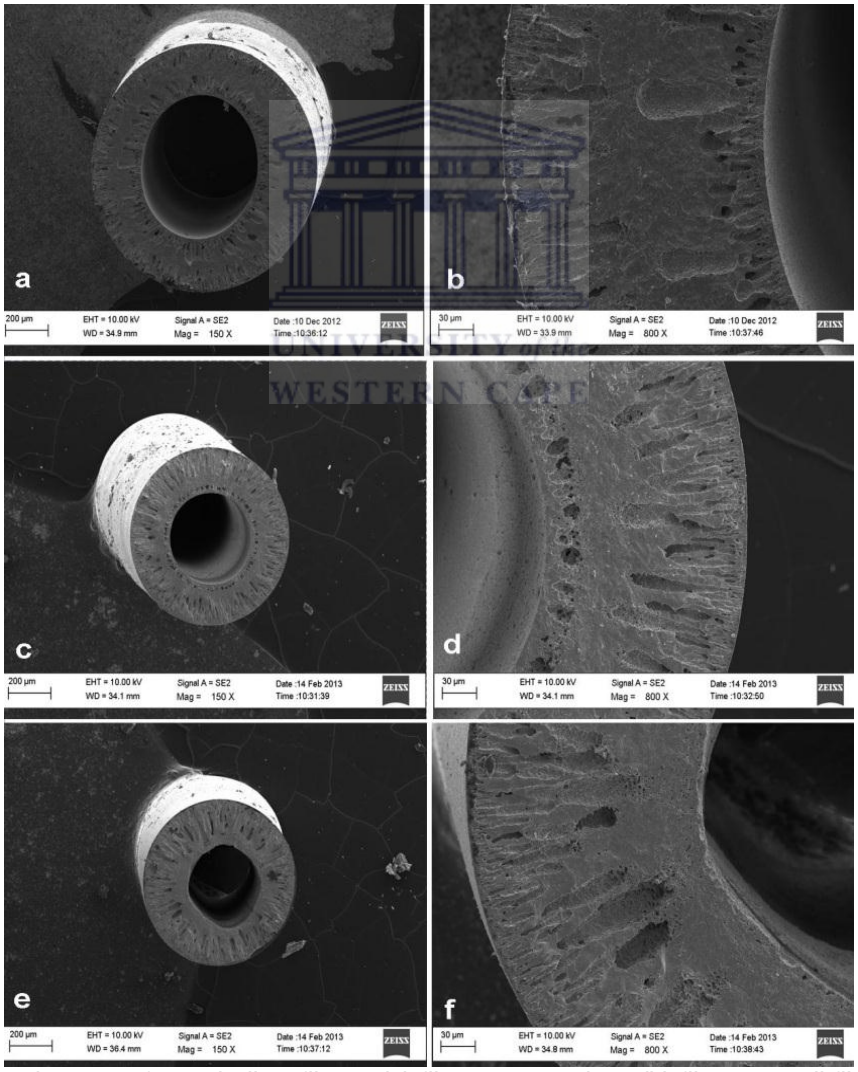

Figure 4.16 SEM images of YSZ hollow fibres: (a) fibre1A, overview; (b) fibre1A, wall fibre; (c) fibre1B, overview; (d) fibre1B, wall fibre; (e) fibre1C, overview;
(f) fibre1C, wall fibre

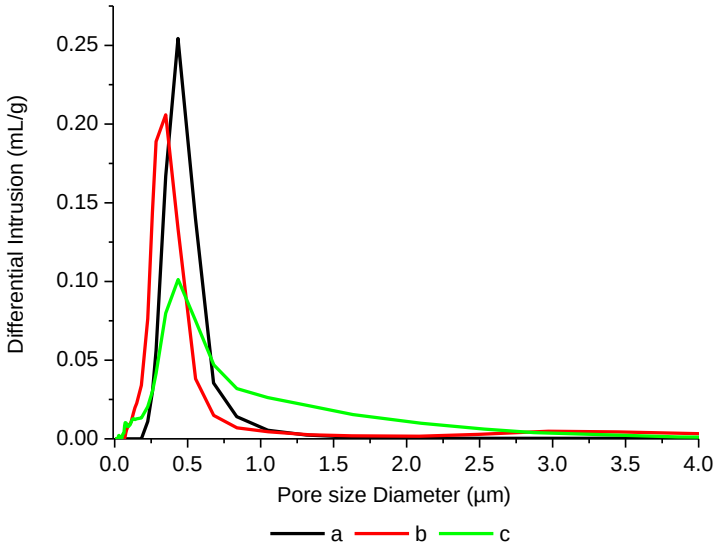

Figure 4.17 Pore size distribution of YSZ supports: internal/external coagulant, (a) $100H_2O/100H_2O$, (b) $60NMP:40H_2O/100H_2O$, (c) $90NMP:10H_2O/100H_2O$

Mercury intrusion data studies of the hollow fibre membranes showed that the pore size distribution of all samples were narrow with a few pores found on both sides of the sharp peak, Fig 4.17. The effects of the internal coagulation on the gas permeance are shown in Fig 4.18. There was found to be a linear relationship between the pressure and air permeability. The gas permeation results indicated that the porosity decreased as NMP concentration in the internal coagulation bath was increased. Such results are in agreement with SEM images shown in Fig 4.16 and mercury data shown in Fig 4.17. The outer surface of the hollow fibre membrane (also depicted in Fig 4.18) is also found to be affected by variation of the internal coagulant.

The outer surface of hollow fibre prepared from F1A (Fig 4.18a) has a fewer number of defects. The likely reason is that coagulation occurred faster when pure water was used as the internal coagulant, leaving very short time for nascent hollow fibre membrane to shrink. But the increase of NMP content at the internal coagulant slowed down the coagulation rate, which allowed longer time for shrinkage resulting in defects (Fig 4.18b-c). Also, it can be clearly seen from the SEM images that increasing the NMP content to 60% gives fibres more irregular inner pores and that pore size of the inner surface of the fibres becomes even bigger with further increase in NMP content (Fig 4.19a-c). The decrease in porosity with increased coagulant is confirmed by results obtained by Deshmukh and Li [134].

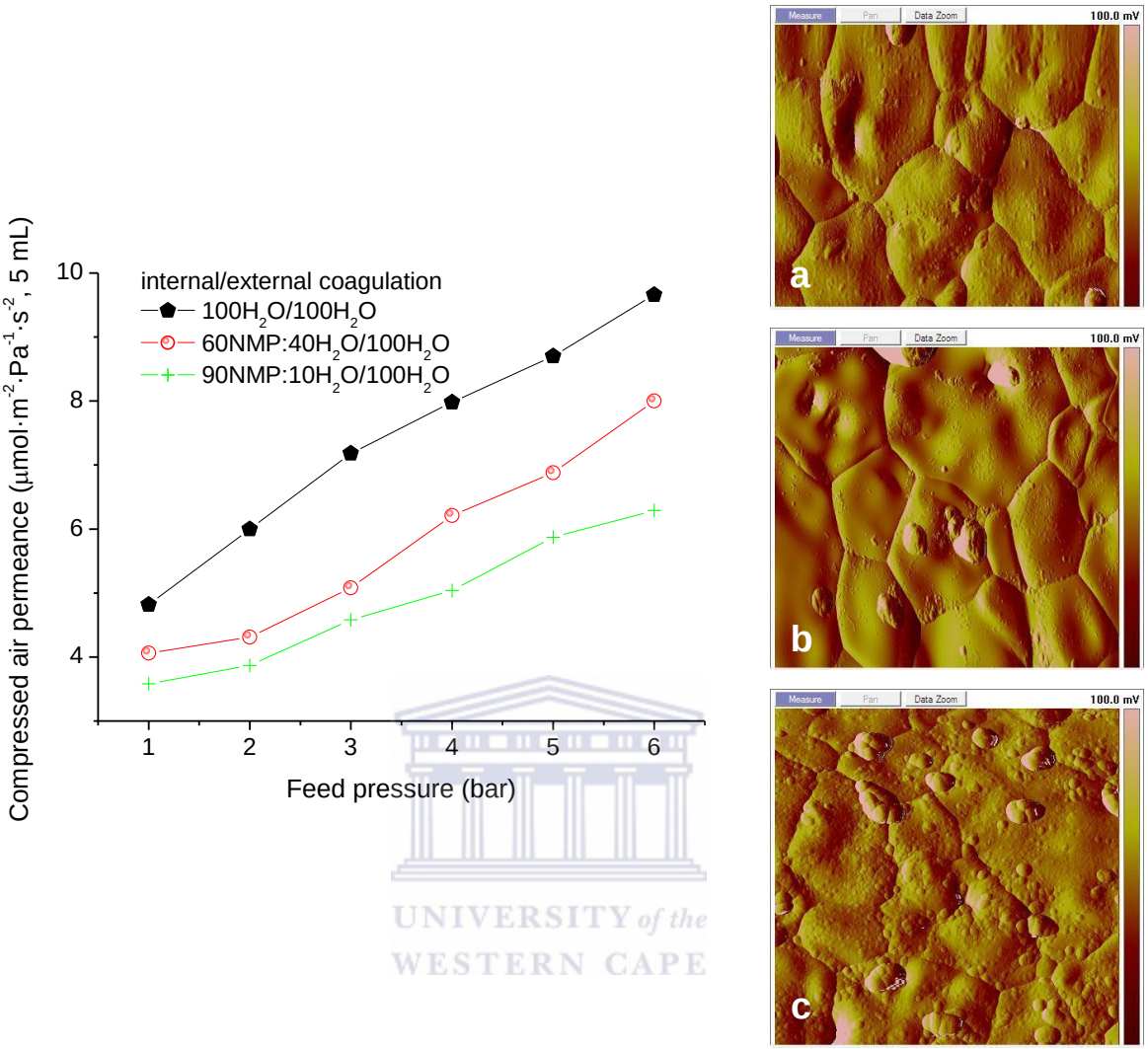

Figure 4.18 Gas permeance of the YSZ hollow fibre prepared at different internal coagulants; (a) $100H_2O/100H_2O$, (b) $60NMP:40H_2O/100H_2O$ and (c) $90NMP:10H_2O/100H_2O$

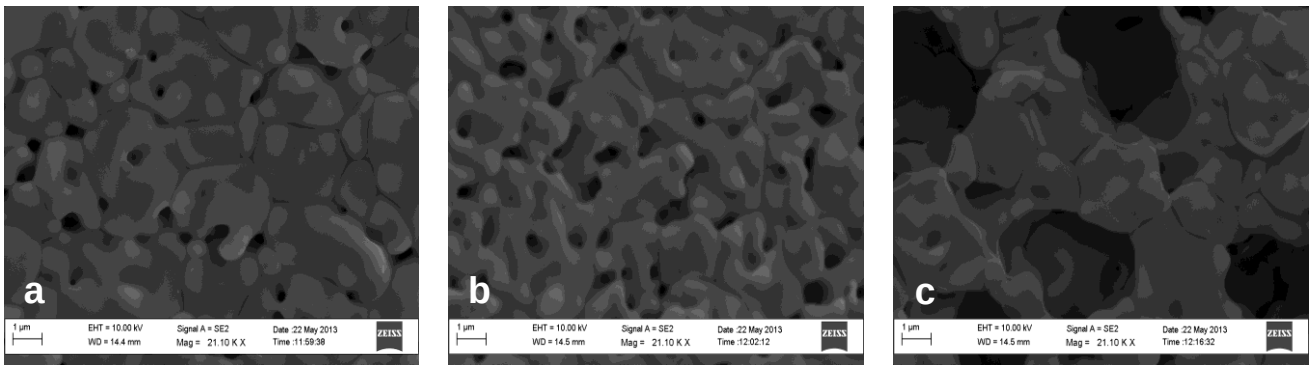

Figure 4. 19 SEM images of the inner surface of YSZ hollow fibre spun at different internal coagulants; (a) $100H_2O/100H_2O$, (b) $60NMP:40H_2O/100H_2O$ and (c) $90NMP:10H_2O/100H_2O$

Chapter 5

5.1 Conclusion

YSZ hollow fibre membranes which have symmetric and asymmetric structure were successfully produced in one step fabrication. The influences of the various spinning parameters, including air gap, bore liquid flow rate, pressure, spinning suspension viscosity, sintering temperature and internal coagulant were investigated. The experiment commenced by examining the particle size of YSZ. From the zetasizer tests, it was noted that at 15 minutes the ultrasonic bath very effectively homogenise the YSZ particles and prohibit soft agglomerates from reforming in the spinning suspension. Experimental results showed that finger-like voids, hollow fibre diameter and wall thickness could be controlled by controlling the spinning parameters.

An increase in air gap had no noticeable effect on the finger like voids but it had a considerable effect on both the ID and OD of the green fibres, while an increase in bore liquid flow rate and extrusion pressure promoted viscous fingering and significant effect on the ID and OD of the fibres, respectively. Supports sintered at higher temperature showed dense structure. Addition of water concentration in the spinning suspension and varying NMP aqueous solution of the internal coagulant resulted in supports with sponge-like structure.

The concentration of YSZ added to the starting suspension influenced the properties of the support structure. Viscous deformation was observed for spinning suspension with lower particle loading thus resulted in the formation of cracks and defects during sintering. Permeation and mercury porosimetry results shows that, by controlling the NMP/water weight ratio of the internal/external coagulant, varying the viscosity of the spinning suspension by using water as an additive and sintering at elevated temperature, gas tight symmetric YSZ hollow fibre membranes can be obtained.

5.2 Recommendations

Several additional studies have been found similar to the analysis of this research experiment. Throughout the course of this study, questions about the utilization of accuracy of the sonication method have been uncovered. It is recommended that spinning suspension in the sonication bath be continually monitored as a means to determine agglomerates effect on the sample. A study focusing on the temperature of the spinning suspension while stirring is suggested.

It seems likely that the porosity is linked to the tensile strength, therefore studies of the effect of mechanical strength could yield some useful correlations.

Future studies should be conducted to investigate the effect of using NMP as the external coagulant for gellation of the extruded hollow fibre precursors with an adjustable crank, preferable few meters deep.

Optimum conditions for plating process on the surface of YSZ hollow fibre membrane to produce very high hydrogen selectivity and permeation rate should be further investigated.

Bibliography

1. Li, K., ***Ceramic Membranes for Separation and Reaction****. John Wiley & Sons, Ltd, Chichester*, 2007: p. 21–131.
2. Diogo, M., Vania, C., Ju-Meng, Z., Silvano, T., Fabio, B., Adelio, M., Luis, M. M., *Int. J. Hydrogen Energy*, 2010. **35**: p. 12596–12608.
3. Li, A., Grace, J. R., Jim Lim, C., *J. Mem. Sci*, 2007. **306**: p. 159–165.
4. Chen, W.H., Chiu, T. W., Hung, C. I., Lin, M. L., *J. Power Sources*, 2009. **194**: p. 467–477.
5. Gao, J., Guo, J., Liang, D., Hou, Z., Fei, J., Zheng, X., *Int. J. Hydrogen Energy*, 2008. **33**: p. 5493–5500.
6. Wei-Hsi, C., Po-Chih, H., *Int. J. Hydrogen Energy*, 2011. **36**: p. 9355–9366.
7. Chen, W.H., Lin, B. C. , *Int. J. Hydrogen Energy*, 2010. **35**: p. 1987–1997.
8. Miguel, V.C., Mendes, A., Tosti, S., Madeira, L. M., *Int. J. Hydrogen Energy*, 2012. **37**: p. 12680–12687.
9. Prabhu, A.K., Ted Oyama, S., *J. Membr. Sci*, 2000. **176**: p. 233–248.
10. Shin-Kun, R., Nong, X., Anwu, L., Jim Lim, C., Grace, J. R., *Int. J. Hydrogen Energy*, 2010. **35**: p. 2328–2335.
11. Li, Y., Y., Nomura, B., Sakoda, A., Suzuki, M., *J. Membr. Sci* 2002. **197**: p. 23–35.
12. Tan, X., Liu, S., Li, K., *J. Membr. Sci*, 2001. **188**: p. 87–95.
13. Baker, R.W., ***Membrane Technology and Application****. John Wiley & Sons, Ltd, Menlo Park, 2nd Ed*, 2004: p. 1–545.
14. Sondhi, R., Bhave, R., Jung, G., ***Membrane Technology****.* 2003: p. 1–5.
15. Pabby, A.K., Rizvi, S. S. H., Sastre, A. M., ***Handbook of Membrane Separation****. U.S*, 2009.
16. Sun, B.G., Hidajat, K., Kawi, S., *J. Membr. Sci*, 2006. **284**: p. 110–119.
17. Consonni, S., Vigano, F., *Int. J. Hydrogen Energy*, 2005. **34**: p. 701–718.
18. Gambini, M., Vellini, M., *Int. J. Hydrogen Energy*, 2005. **30**: p. 593–604.
19. Lu, G.Q., Diniz da Costa, J. C., Duke, M., Giessler, S., Socolow, R., Williams, R. H., Kreutz, T., *J. Colloid Interface Sci*, 2007. **314**: p. 587–603.
20. Meinema, H.A., Dirrix, R. W. J., Brinkman, R. A., Terpstra, R. A., Jekerle, J., Kosters, P. H., *High Perfomance Ceramics*, 2005. **54**: p. 86–91.
21. Song, C., Schobert, H. H. , Fuel, 1996. **75** (6): p. 724–736.
22. Gestel, T., Sebold, D., Wilhelm, A. M., Bram, M., Buckremer, H-P., *Solid State Ionics*, 2008. **179**: p. 1360–1366.

23. Liu, S., Li, K., Hughes, R., *Ceram. Int*, 2003. **29**: p. 875–881.
24. Su, J.O., Kim, N., Lee, Y. T. , *J. Membr. Sci*, 2009. **345**: p. 13–20.
25. Smid, J., Avci, C.G., Gunay, V., Terpstra, R. A., Van Eijk, J.P.G.M., *J. Membr. Sci* 1996. **112**: p. 85–90
26. Tan, X., Li., K., *Curr. Opin. Chem. Eng*, 2011. **1**: p. 69–76.
27. Bai, C., Jia, M., Falconer, J. L., Noble, R. D., *J. Membr. Sci* 1995. **105**(1–2): p. 79–87.
28. Li, A., Liang, W., Hughes, R., *Catal. Today*, 2000. **56**: p. 45–51.
29. Bryden, J.K., Ying. Y. J., *J. Membr. Sci*, 2002. **203**: p. 29–42.
30. Shiga, H., Shinda, K., Hagiwara, K., Tsutsumi, A., Sakurai, M., Yoshida, K., Bilgen, E., *Int. J. Hydrogen Energy*, 1998. **23**: p. 631–640.
31. Ramachandran, R., Menon, K. R., *Int. J. Hydrogen Energy*, 1998. **23**: p. 593–598.
32. Rosen, A.M., Scott, S. D., *Int. J. Hydrogen Energy*, 1998. **23**: p. 653–659.
33. Kikuchi, E., *Catal. Today*, 2000. **56**: p. 97–101.
34. Burkhanov, S.G., Gorina, B. N., Kolchugina, B. N., Roshan, R. N., *Platinum Metals Rev*, 2011. **55**: p. 3–12.
35. Hunter, J.B., *Platinum Met. Rev*, 1960. **4**(4): p. 130–131.
36. Grashoff, G.J., Pilkington, C. E.,Corti, C. W., *Platinum Met. Rev*, 1986. **30**: p. 157.
37. Xomeritakisa, G., Tsai, C. Y., Jiang, Y. B., Brinkera, C. J., *J. Membr. Sci* 2009. **341**: p. 30–36.
38. Jang, S.K., Kim, H. J., Johnson, J. R., Kim, W., Koros, W. J., Jones, W. C., Nair, S., *Chem. Mater*, 2011. **23**: p. 3025–3028.
39. Stanislowski, J.J., Laumb, J.D., ***Gasification of Lignites to Produce Liquid Fuels****. Hydrogen and Power, Pittsburgh Coal*, 2009.
40. Sammells, F.A., Mundschau, V. M., ***Nonporous Inorganic Membranes for Chemical Processing****. WILEY-VCH Verlag GmbH & Co. KGaA, Weinheim*, 2006: p. 77–82.
41. Khatib, S.J., Oyama, S. T., *Sep. Purif. Technol*, 2013. **111**: p. 20.
42. Cuperus, F.P., Bargeman, D., Smolders, C. A., *J. Membr. Sci*, 1992. **66**(1): p. 45–53.
43. Askeland, D.R., Fulay, P. P., Wright W. J., ***The Science and Engineering of Materials****. Cengage Learning, Inc, 6th Ed*, 2010: p. 8–9.
44. Nam, E.S., Lee, H. K., *J. Membr. Sci*, 2001. **192**: p. 177–185.
45. Mardilovich, I.P., She, Y., Ma, Y. H., Rei, M. H., *AIChE J*, 1998. **44**: p. 310–322.
46. Uemiya, S., Endo, T., Yoshiie, R., Katoh, W., Kojima, T., *Mater. Trans*, 2007. **48**: p. 1119–1123.
47. Qiao, A., Zhang, K., Tian, Y., Xie, L., Luo, H., Lin, Y.S., Li, Y., *Fuel*, 2010. **89**: p. 1274–1279.

48. Paglieri, S.N., Way, J. D., *Sep. Purif. Rev*, 2002. **31**: p. 1–169.
49. Wang, D., Tong, J., Xub, H., Matsumura, Y., *Catal. Today*, 2004. **93–95**: p. 689–693.
50. Mardilovich, I.P., Ma, E. S., Engwall, Y. H. , *Desalination*, 2002 **144**: p. 85–89
51. Shu, J., Adnot, A., Grandjean, B. P. A., Kaliaguine, S., *Thin Solid Films*, 1996. **286**: p. 72–79.
52. Jemaa, N., Shu, J., Kaliaguine, S., Grandjean, P. A., *Ind. Eng. Chem. Res*, 1996. **35**: p. 973–977.
53. Amandusson, H., Ekedahl, G. L., Dannetun, H., *J. Membr. Sci*, 2001. **193**: p. 35–47.
54. Cochran, J.K., *Curr. Opin in Solid State & Material Science*, 1998. **3**: p. 474–479.
55. Liu, H., Tan X., Pang, Z., Diniz da Costa, J. C., Lu, G, Q., Liu, S., *Sep. Purif. Technol*, 2008. **63**: p. 243–247.
56. Benjamin, F.K., Li, K. K., *J. Membr. Sci*, 2009. **328**: p. 134–140.
57. Zhang, X., Lin, B., Ling, Y., Dong, Y., Fang, D., Meng, G., Liu, X., *J. Alloys Compd*, 2010. **494**: p. 366–371.
58. Benito, J.M., Conesa, A., Rubio, F., Rodriguez, M. A., *J. Eur. Ceramic. Soc*, 2005. **25**: p. 1895–1903.
59. Collins, J.P., Schwartz, R. W., Sehgal, R., Ward, T. L., Brinker, C. J., Hagen, G. P., Udovich, C. A. , *Ind. Eng. Chem. Res*, 1996. **35**(12): p. 4398–4405.
60. *Hydrogen Association (website). http://www.hydrogenassociation.org/general/faqs.asp.* [Accessed 27 May 2013].
61. Javaid, A., *Chem. Eng. J*, 2005. **112**: p. 219–226.
62. Paul, D.R., Morel, G., ***In: Kirh-othmer Encyclopedia of Chemical Technology***. *John wiley & Sons, INC, 3rd Ed, vol 15*, 1980.
63. Wei, C.C., Chen, O. Y., Liu, Y., Li, K., *J. Membr. Sci*, 2008. **320**: p. 191–197.
64. Singh, B., Sheth, A. C., Dahotre, N. B., *Appl. Surf. Sci*, 2006. **253**: p. 1247–1254.
65. David, E., Kopac, J., *Int. J. Hydrogen Energy*, 2011. **36**: p. 4498–4506.
66. Ulbricht, M., *Polymer* 2006. **47**: p. 2217–2262.
67. Wei, C.C., Li, K., *Ind. Eng. Chem. Res*, 2008. **47**: p. 1506–1512.
68. Laosiripojana, N., Assabumrungrat, S., *J. Power Sources*, 2007. **163**: p. 943–951.
69. Razmjou, A., Resosudarmo, A., Holmes, R. L., Li, H., Mansouri, J., Chen, V., *Desalination*, 2012. **287**: p. 271–280.
70. Luiten-Olieman, M.W.J., Raaijmakers, M. J. T., Winnubst, L., Bor, T. C., Wessling, M., Nijmeijer, A., Benes, N. E., *J. Mem. Sci*, 2012. **407– 408** p. 155–163.
71. Pan, L.X., Stroh, N., Brunner, H., Xiong, X. G., Sheng, S. S., *Chem.Commun*, 2001.(24): p. 2536–2537.
72. Okazaki, J., Ikeda, T., Pacheco Tanaka, D. A., Llosa Tanco, M. A., Wakui, Y., Sato, K., Mizukami, F., Suzuki, T. M., *Chem. Lett*, 2008. **37**(9): p. 1004–1005.

73. Gestel, T., Sebold, D., Kruidhof, H., Bouwmeester, H. J. M., *J. Membr. Sci*, 2008. **318**: p. 413–421.
74. Wei, L., Jian-Jun, L., Chu-Sheng, C., *J. Mem. Sci*, 2009. **340**: p. 266–271.
75. Yang, C., Li, W., Zhang, S., Bi, L., Peng, R., Chen, C., Liu, W., *J. Power Sources*, 2009. **187**: p. 90–92.
76. Cheng, S.Y., Peña, A. M., Fierro, L. J., Hui, W. C. D., Yeung, L. K., *J. Membr. Sci*, 2002. **204**: p. 329–340.
77. Peachey, M.N., Snow, C. R., Dye, C. R., *J. Membr. Sci*, 1996. **1**: p. 123–133.
78. Pan, L.X., Stroh, N., Brunner, H., Xiong, X. G., Sheng, S. S., *Sep. Purif. Technol*, 2003. **32**: p. 265–270.
79. Leenaars, A.F.M., Burggraaf, A. J., *J. Colloid Interface Sci*, 1985. **105** (1): p. 27–40.
80. Uhlhorn, R.J.R., Veld, M., Keizer, K., Burggraaf, A. J., *J. Mater. Sci. Lett*, 1989. **8**(10): p. 1135–1138.
81. Tiller, F.M., Tsai, C. D., *J. Am. Ceram. Soc*, 1986. **69**(12): p. 882–887.
82. Barlow, F.D., Elshabini, A., ***Ceramic Interconnect Technology Handbook***. *Taylor & Francis Group, LLC*, 2007: p. 163–196.
83. Boaro, M., Vohs, J. M., Gorte, R. J., *J. Am. Ceram. Soc*, 2003. **86**(3): p. 395–400.
84. Xia, C., Liu, M., *J. Am. Ceram. Soc*, 2001. **84**(8): p. 1903–1905.
85. Iwata, M., Adachi, T., Tomidokoro, M., Ohta, M., Kobayashi, T., *J. Appl. Polym. Sci*, 2003. **88**: p. 1752–1759.
86. Buckley, A.M., Greenblatt, M., *J. Non-Cryst. Solids*, 1996. **8**: p. 1682–1701.
87. Baker, G.A., Pandey, S., Maziarz, E. P., Bright, F. V., *J. Sol-Gel Sci. Technol*, 1999. **15**: p. 37.
88. Javaids, A., *Chem. Eng. J*, 2005. **112**: p. 219–226.
89. Yoshimune, M., Haraya, K., *Sep. Purif. Technol*, 2010. **75**: p. 193–197.
90. Wei, C.C., Li, K., *Ind. Eng. Chem. Res*, 2009. **48**: p. 3446–3452.
91. Li, K., Tan, X., Liu, Y., *J. Membr. Sci*, 2006. **272**: p. 1–5.
92. Liu, S., Li, K., *J. Membr. Sci*, 2003. **218**: p. 269–277.
93. Liu, S., Tan, X., Li, K., Hughes, R., *J. Membr. Sci*, 2001. **193**: p. 249–260.
94. Liu, S., Li, K., Hughes, R., *Mater. Res. Bulletin*, 2004. **39**(1): p. 119–133.
95. Hseih, H.P., *Elsevier Science B.V*, 1996: p. 23–86.
96. Gonzalo-Juan, I., Ferrari, B., Colomer, M. T., Rodriguez, M. A., Sanchez-Herencia, A. J., Koh, P. Y., Teja, A. S., *Mater. Chem. Phys*, 2012. **134**: p. 451– 458.
97. Cao, X., Ma, J., Shi, X., Ren, Z., *Appl. Surf. Sci*, 2006. **253**: p. 2003–2010.
98. Wang, D., Li, K., Teo, W. K., *J. Membr. Sci* 2000. **166**: p. 31–39.
99. De Jong, J.B., N. E., Koops, G. H., Wessling, M., *J. Membr. Sci*, 2004. **239**: p. 265–269.

100. Li, S.G., Koops, M. H. V., Van den Boomgaard, T. M., Smolders, C. A., *J. Mem. Sci*, 1994. **94**: p. 329–340.
101. Machado, P.S.T., Habert, A.C., Borges, C.P., *J. Membr. Sci*, 1999. **155**: p. 171–183.
102. Smolders, C.A., Reuvers, A. J., Boom, R. M., Wienk, I. M., *J. Membr. Sci*, 1992. **73**: p. 359–275.
103. Young, T., Chen, L., *Desalination*, 1995. **103**: p. 223–247.
104. Cabasso, I., ***Encyclopedia of chemical technology***. *John Wiley & Sons, NC, 3rd Ed, Vol.12*, 1980.
105. Bergstrom, L., *J. Am. Ceram. Soc*, 1996. **79**(12): p. 3033–3040.
106. Luiten-Olieman, M.W.J., Raaijmakers, M. J. T., Winnubst, L., Bor, T. C., Wessling, M., Nijmeijer, A., Benes, N. E., *J. Mem. Sci*, 2011. **370**: p. 124–130.
107. Aptel, P., Abidine, N., Ivaldi, F., Lafaille, J. P., *J. Membr. Sci*, 1985. **22**: p. 199–215.
108. East, G.C., McIntyre, J. E., Rogers, V., Senn, S. C., ***Production of porous hollow fibre polysulfone fibers for gas separation***. *Royal Society of Chemistry, London*, 1986: p. 63.
109. Liu, T., Zhang, D., Xu, S., Sourirajan, S., *Sep. Sci. Technol*, 1992. **27**: p. 161–174.
110. Clause, D.T.a.K., W.J., *J. Membr. Sci*, 2000. **167**: p. 79–89.
111. Lin, Y.S., de Vries, K. J., Burggraaf, A. J., *J. Mater. Sci*, 1991. **26**: p. 715.
112. Levanen, E., Kolari, M., Mantyla, T., *The symposium of the ICIM'3, Worcestor*, 1994: p. 549–552.
113. Wang, P., Huang, P., Xu, N., Shi, J., Lin, Y. S., *J. Membr. Sci*, 1999. **155**: p. 309–314.
114. Khayet, M., Matsuura, T., *Desalination*, 2003. **158** p. 57–64.
115. Chhabra, R.P., Richardson, J. F., 2008, ***Non-Newtonian flow and applied rheology***. *2nd edn.* Butterworth-Heinemann, Oxford.
116. Mulder, M., ***Basic Principle of Membrane Technology***. *Kluwer Academic Publishers, Dordrecht, 1st Ed,* 2000.
117. Mulder, M., ***Basic Principle of Membrane Technology***. *Kluwer Academic Publishers, Dordrecht, 2nd Ed,* 1996.
118. Jena, A., Gupta, K., *Porous Mateials Inc*, 2001: p. 1–11.
119. Barth, C., Gonçalves, M. C., Pires, A. T. N., Roeder, J., Wolf, B. A., *J. Mater. Sci*, 2000. **169**: p. 287–299.
120. Wang, D., Li, K., Teo, W. K., *J. Membr. Sci*, 2002. **204**: p. 247–256.
121. Chung, T.S., Hu, X., *J. Appl. Polym. Sci*, 1997. **66**: p. 1067–1077.
122. Ismail, A.F., Suhaina, M. I., Nasri, N. S., *J. Sci. Technol*, 2002. **24**: p. 833–842.
123. Shilton, S.J., Bell, G., Ferguson, J., *Polymer*, 1994. **35**: p. 5327–5335.
124. Shilton, S.J., Bell, G., Ferguson, J., *Polymer*, 1996. **37**: p. 485–492.

125. Strathmann, H., *Desalination*, 1977. **21**: p. 241–255.
126. Singh, S., Khulbe, K. C., Matsuura, T., Ramamuthy, P. , *J. Membr. Sci*, 1998. **142**: p. 111.
127. Bessieres, A., Meireles, M., Cortger, R., Beavillain, J., Sanchez, V., *J. Membr. Sci*, 1996. **109**: p. 271.
128. Fritzche, A.K., Arevalo, A. R., Moor, M. D., Weber, C. J., Elings, V. B., Kjoller, K., Wu, M. C., *J. Appl. Polym. Sci*, 1992. **46**: p. 167.
129. Vrijenhoek, E.M., Hong, S., Elimelech, M., *J. Mem. Sci*, 2001. **188**: p. 115–128.
130. Jayaseelan, D., Ueno, S., Ohji, T., Kanzaki, S., *Sci. Adv. Mater*, 2004. **5**: p. 387.
131. García-García, F.R., Kingsbury, B. F. K., Rahman, M. A., Li, K., *Catal. Today*, 2012: p. 1–11.
132. Kesting, R.E., ***Synthetic Polymeric Membranes***. *New York, Wiley, 2nd Ed*, 1985: p. 237–261.
133. Wang, D., Li, K., Teo, W.K., *J. Membr. Sci* 1999. **163**: p. 211–220.
134. Deshmukh, S.P., Li, K., *J. Mem. Sci*, 1998. **150**: p. 75–85.